Jukka Syrjämäki

5V POWER SUPPLY SUITABLE FOR ALL AC

MOTORS

ABB LTD, Motors & Generators

This is a translation of the original Finnish version. In case of ambiguity, refer to the original thesis document.

School of Technology
2021

VAASA UNIVERSITY OF APPLIED SCIENCES
Electrical engineering

ABSTRACT

Author	Jukka Syrjämäki
Title	5V Power Supply Suitable for All Motors
Year	2021
Language	English
Pages	58 + 4 Appendices
Name of Supervisor	Marko Iskala

The topic of this thesis was to build a 5 V power supply suitable for all motors. This thesis was made for the R&D department of ABB Motors & Generators in Vaasa. The main aim was to find a way to transform frequency converter output voltage into a clean DC voltage of desired amplitude, or harvest energy from another source, such as vibration or magnetic fields into electrical energy.

After reviewing the feeding solutions, the most promising option was selected for closer examination. The implementation of this solution was examined by simulating different operating situations with PSCAD and comparing the results. After the simulation phase, the solution was tested in the testing field and the actual behaviour of the device was compared with the simulated results.

Finally, the operation of this solution was evaluated based on tests, as well as its suitability for the intended use. A prototype of one development idea was also built and briefly tested the same way as the original device. Additionally, development ideas and options on how to proceed with the project are presented in the thesis.

TABLE OF CONTENTS

LIST OF FIGURES

LIST OF TABLES

APPENDICES

APPENDIX 1. WDR-60-5 power supply fed with sine voltage.

APPENDIX 2. WDR-60-5 power supply fed with a frequency converter.

APPENDIX 3. WDR-60-5 power supply fed with a frequency converter, in parallel with a motor.

APPENDIX 4. Simulated switching logic of the improved frequency converter.

ABBREVIATIONS

R&D	Research & Development
CVT	Capacitor voltage transformer
AC	Alternating current
DC	Direct current
I_p	Primary current
I_s	Secondary current
N_s	Number of turns in secondary winding
$I_{m,s}$	Magnetizing current in secondary winding
I_L	Current taken by the load
U_s	Secondary voltage
R_L	Load resistance
$L_{m,s}$	Magnetizing inductance in secondary winding
ω	Angular frequency ($2\pi f$)
P_L	Power delivered to the load
μ_0	Vacuum permeability
μ_r	Relative permeability
A_e	Area of iron core
D	Diameter
EMI	Electro-Magnetic Interference
V	Volt
A	Ampere

W	Watt
PWM	Pulse Width Modulation
DTC	Direct Torque Control
PSCAD	Power Systems Computer Aided Design
R1	Resistance of NTC-thermistor in temperature T1
R2	Resistance of NTC-thermistor in temperature T2
T1	First temperature, from NTC-thermistors datasheet /13/
T2	Second temperature, from NTC-thermistors datasheet /13/
β	Temperature coefficient of NTC-thermistor
Hz	Hertz
NTC	Negative Temperature Coefficient
Vp-p	Voltage peak to peak
mAp-p	Milliamperes peak to peak
Pn	Nominal power
U1	Input voltage
U2	Output voltage
I1	Input current
I2	Output current
f1	Input frequency
f2	Output frequency

1   INTRODUCTION

This thesis is made for the R&D department of ABB Motors & Generators in Vaasa. The aim of the work is to build a 5 V 1 A DC output suitable for all AC motors. Alternative solutions to implement the device in question are examined, after which electrical studies are continued by simulating different operating situations. The device will be tested on the test field after the simulations have given an idea of how the solution works.

The idea behind a 5 V output device suitable for electric motors is that any peripherals could be powered directly from the motor and therefore no separate supply would be needed. One example of such peripherals is the ABB Ability Smart Sensor, which can be used to monitor motor condition and detect potential problems before they cause any greater damage. At the same time, this would also provide the ability to supply third-party equipment.

The requirement for the device is a wide voltage range for the supply, it must also work on frequency converter driven motors, and the device should be as small and compact as possible. A wide voltage range ensures that the device works anywhere the motor is used and regardless of the connection. The ability of the device to operate when fed with a frequency converter also ensures that it works on all motors. The physical size of the device, on the other hand, should be small so it could be sensibly added to smaller motors as well, for example, in a separate terminal box.

2   ABB LTD.

ABB Oy is a global technology company in robotics, automation and power technology areas. ABB LTD was formed in the year 1988, when the Swedish ASEA (founded in 1883) and Swiss Brown, Boveri & Cie (founded in 1891) merged. ASEA's production sector at the time was electric lamps and generators, while Brown, Boveri & Cie manufactured AC and DC motors, generators, steam turbines and transformers. Today, ABB, led by Björn Rosengren, is divided into four industries: Electrification, Process Automation, Motion and Robotics & Discrete Automation. Electrification includes, among other things, smart electrification options for industry, housing and electricity distribution. Process automation offers solutions for measurement and analytics systems, control systems and programmable logic controllers. Motion includes drives, motors, generators and mechanical gears. Robotics & Discrete Automation offers solutions in robotics, as well as machine and factory automation. /1,2/

In Finland, ABB's position is based on Oy Strömberg Ab, an electrical engineering company founded by Gottfrid Strömberg in 1889 and transferred to ASEA in 1987. Gottfrid Strömberg manufactured Finland's first DC motor in 1880, graduated from the Polytechnic College in 1885, and learned electrical engineering at the Royal Technical College of Berlin and the Hanover Technical College. Oy Strömberg Ab started its operations at the dynamo factory it founded in Kamppi, Helsinki, in 1891, and by 1917 the manufacturing programme already included DC generators, AC motors, transformers, control cabinets, various breakers, switches, fuses, voltage controllers and entire dashboards in addition to dynamos. In February 1944, Oy Strömberg Ab also started operations in Vaasa, where production was transferred due to the bombings in Helsinki during the Second World War and the Continuation War. /3,4/

3   OPTIONS FOR INPUT METHODS

When designing the electricity supply of the output circuit, energy harvesting methods were first investigated. The energy harvesting methods studied for the thesis include piezoelectric energy harvesting based on mechanical vibration and energy harvesting carried out with a current transformer. In addition to these, systems connected directly to the motor terminals were also examined. The following paragraphs present the results of the investigation and the theory of the above-mentioned means of energy harvesting methods.

3.1 Piezoelectric Energy Harvesting

In piezoelectric energy harvesting, the mechanical vibration is converted into electrical energy. In piezoelectric energy harvesting methods, piezoceramics installed in the motor terminal box and piezoelectric laminates placed around motor cables are considered.

The operating idea of the piezoceramics installed inside the terminal box is to generate electrical energy from the vibration of the motor. Figure 1 shows a comparison of the power densities of piezoelectric and some alternative energy harvesting methods as a function of voltage. Figure 2 shows an example of a piezoceramic charging a thin film battery, as well as the voltage and current that this produces that charges the battery. The main concern of this energy harvesting method to the suitability for the output is: Are the motor vibration levels allowed by the IEC standard sufficient to generate the desired voltage at the output with piezoceramics of the appropriate size for the motor?

In Figure 1, the possible voltage to be achieved by the power supply system is shown on the horizontal axis and the power density in milliwatts per cubic centimeter is shown on the vertical axis. Piezoelectric systems are found to be able to achieve the most extensive power supply in the range of the options presented.
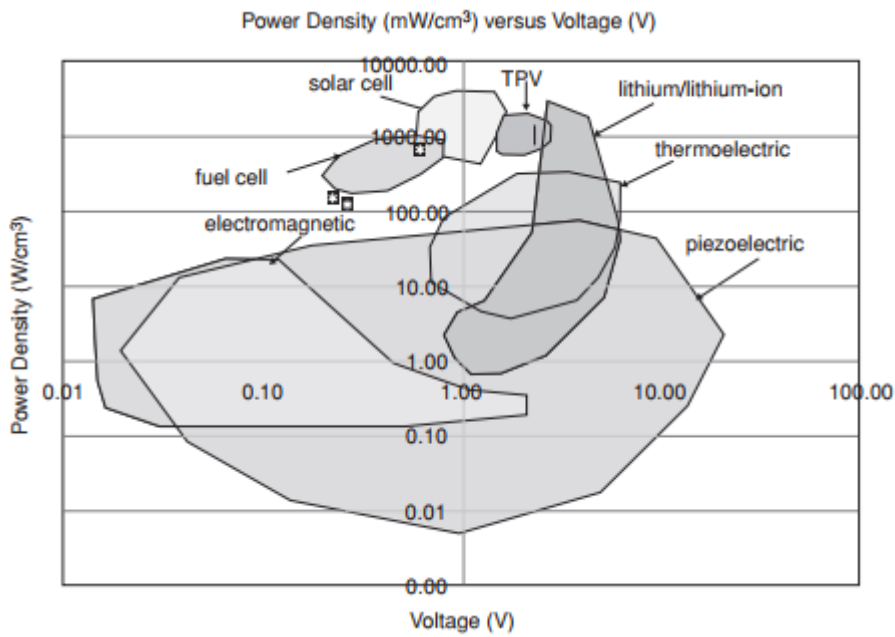
Figure 1. Power densities of renewable and lithium-ion power supply systems as a function of voltage. /5/
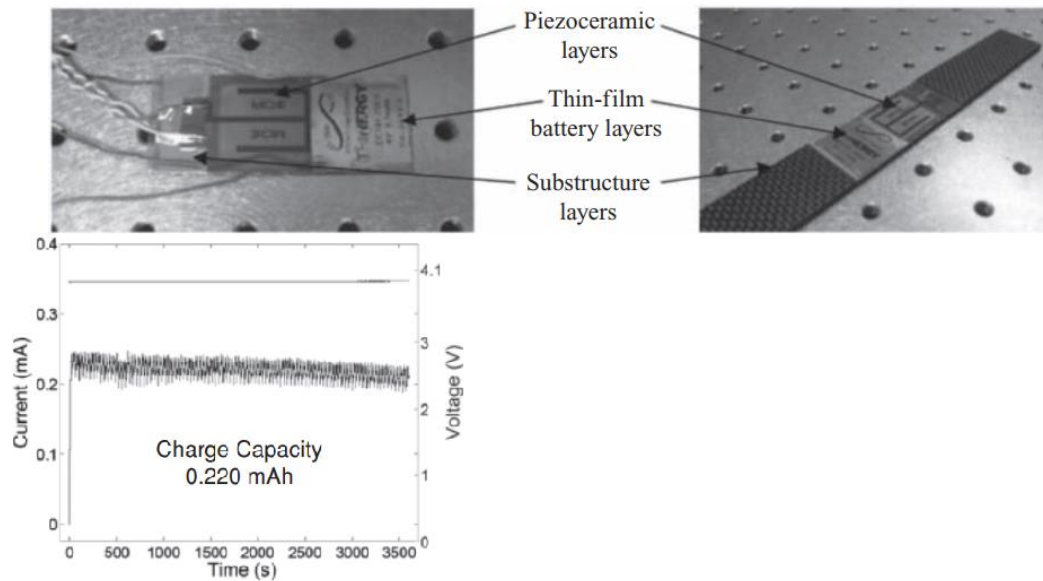
Figure 2. An example of the structure of piezoceramics and the voltage and current generated by this when charging a thin film battery. /5/

According to the figure, a piezoelectric system producing 5-V could achieve a power of just under 90 mW per cubic centimeter of piezoelectric material. This means that the 5 W desired for the output could be achieved with at least 11-cm^{3}of piezoelectric material.

Another piezoelectric option was the flexible laminate wrapped around the motor cable, which generates electrical energy from the magnetic field of the conductors. As shown in Figure 3, the laminate consists of two piezoelectric layers with a magnetostrictive layer between them. This method has been tested in a source study on the power cord of an electric iron in America, i.e. at 60 Hz and 120 V. In this test, the voltage produced by the 267 mm long piezoelectric laminate over a period of 200 ms is shown in Figure 4. /6/

(a)
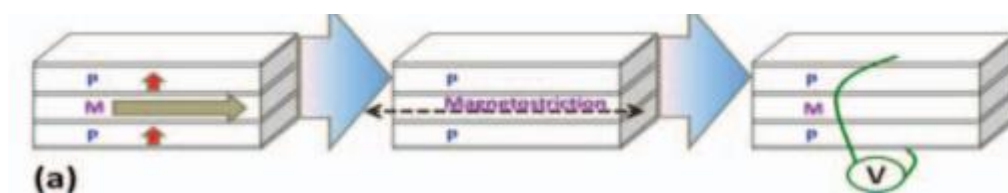
Figure 3. Structure of the flexible piezoelectric laminate. /6/
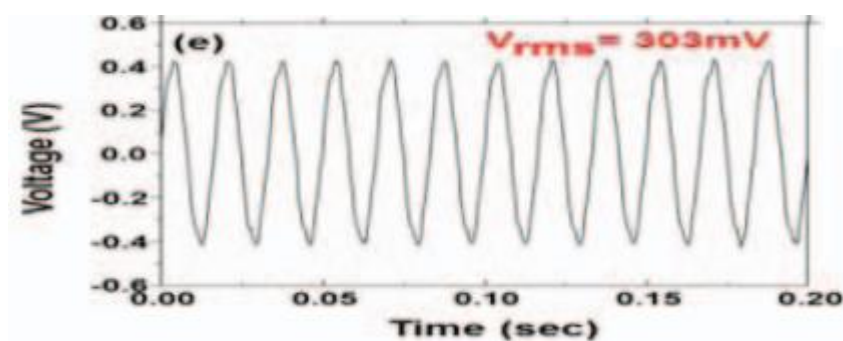
Figure 4. Voltage produced by a 267 mm piezoelectric laminate around the power cord of an electric iron (120 V, 60 Hz). /6/

A closer examination of piezoelectric systems was discontinued at this stage of the project, as they were found to be insufficient to generate enough power to meet the needs of this project, according to Figures 2 and 4.

3.2 Energy Harvesting with a Current Transformer

In this option, the magnetic field in the motor cables is converted into electrical energy by means of a solution based on a current transformer. The iron core of the current transformer consists of two U-shaped bodies forming a toroid coil. The primary side of the current transformer is the motor cable, which is passed directly

through the iron core. The secondary of the current transformer is wound on the other side of iron core. Therefore, the following equation applies to the current values of the current transformer:

$$I_p = N_s * I_s \tag{1}$$

Where I_p is primary current, N_s is the number of turns in secondary winding and I_s is secondary current. The number of turns on primary side here is always 1, since the motor cable is not rotated around the iron core of the current transformer. Secondary current of the current transformer can also be calculated using the following equation:

$$I_s = \sqrt{I_{m,s}^2 + I_L^2} \tag{2}$$

Where $I_{m,s}$ is magnetizing current and I_L is current taken by the load. The equation of secondary voltage is based on the equivalent circuit shown in figure 5. The equation of secondary voltage U_s can now be written as follows:

$$U_s = R_L I_L = \omega L_{m,s} I_{m,s} \tag{3}$$

Where R_L is resistance of the load, $L_{m,s}$ is magnetizing inductance in secondary winding and ω is angular frequency. The equation for power taken by the load P_L can be written as follows:

$$P_L = U_s I_L = \omega L_{m,s} I_{m,s} I_L \tag{4}$$

The magnetization inductance is defined at the design stage and depends on factors such as iron core dimensions, magnetic properties of the core material, density of the flux and number of secondary winding turns. In case of a toroid coil without an airgap, the following equation applies to the magnetizing inductance:

$$L_{m,s} = \frac{\mu_0 \mu_r A_e N_s^2}{\pi D} \tag{5}$$

Where μ_0 and μ_r are vacuum permeability and relative permeability of transformers core material, A_e is surface area of core and D is the diameter from the center of core structure to the opposite side of the center of core structure. Figure 6 shows an example prototype of the current transformer to be built as a power supply, and the estimated power densities as a function of the primary current RMS values in Figure 7. The highest output powers achieved as a function of primary current RMS values are shown in Figure 8. /7/
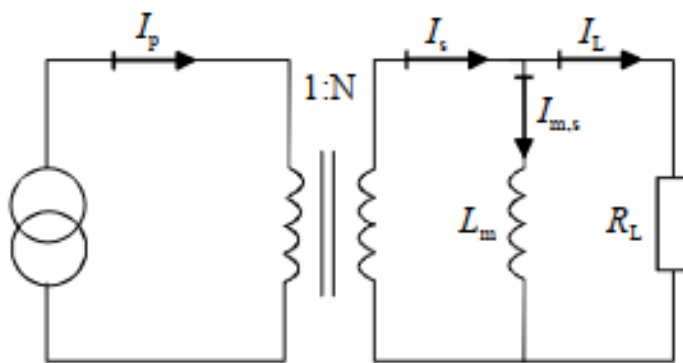
Figure 5. Equivalent circuit of an ideal current transformer /7/

Figure 6. Current transformer installed around the motor phase conductor. /7/
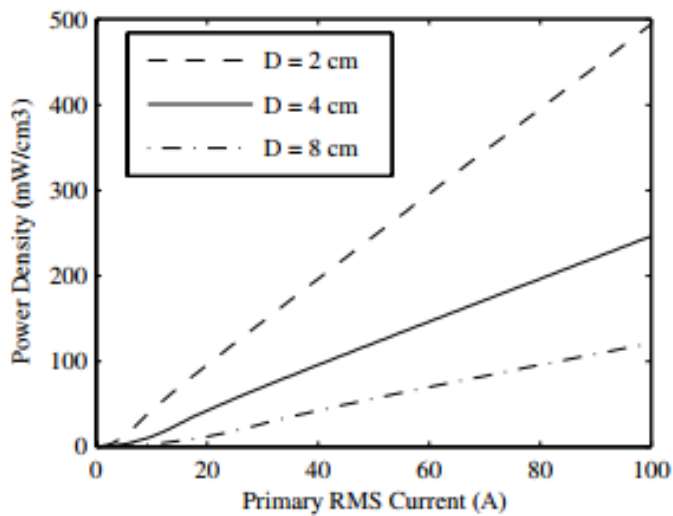
Figure 7. Estimated power densities for current transformer-based supply as a function of the primary current. Graphs for three transformer sizes, where D is the length of the transformer diameter from center to center. /7/
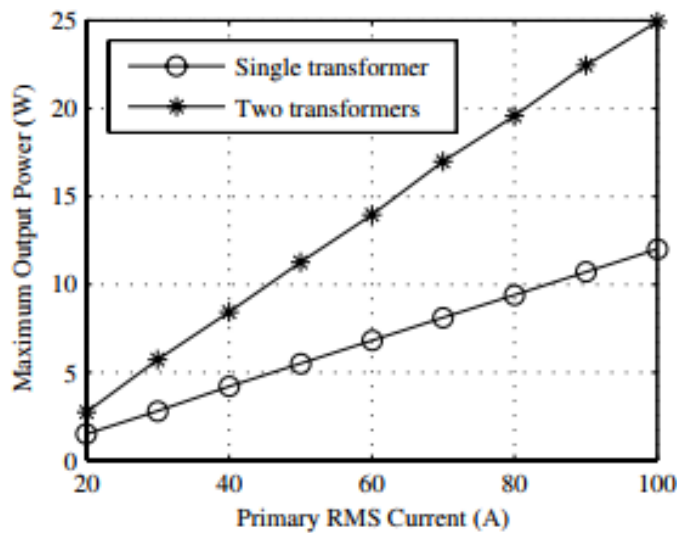
Figure 8. Highest output powers achieved as a function of primary current RMS values. /7/

A closer examination of the current transformer-based systems was discontinued at this stage of the project, as they were found to be insufficient to generate enough power with reasonable primary currents. Based on Figure 8, the target output of the project of 5 W could be achieved with either primary current of

about 50 A, or 25 A when using two current transformers. According to these re-
sults, current transformer-based systems are not suitable, especially for smaller
motors that take much less power than this.

3.3 Capacitor Voltage Transformer (CVT)

In this solution, the output circuit is supplied directly from the motor terminals.
The first part in a CVT is a voltage divider made of capacitors, from which the volt-
age is brought to a transformer to be further reduced. Compared to a standard
transformer, CVT becomes cheaper and usually requires less space thanks to a
smaller transformer /8/. Figure 9 shows the circuit of a simple CVT.
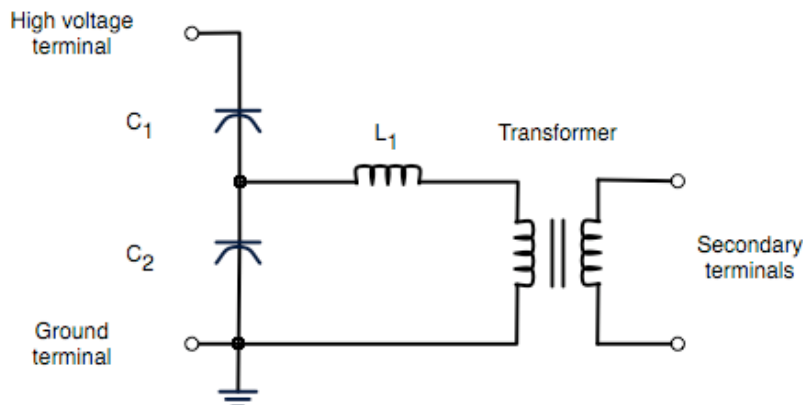
Figure 9. Circuit diagram of a simple CVT. /8/

In the case of this input method, a suitable transformer would first be selected and
the capacitors C1 and C2 shown in Figure 5 would be rated, as well as the coil L1
to compensate for the capacitor reactance. After these, the transformer second-
ary side would need interference filtration circuits, rectifier and regulation to the
voltage range of 4.75 V – 5.25 V that is required by USB-standard /9/.

3.4 An Existing Power Supply (Mean Well WDR-60-5)

The option chosen for further investigation in this project was to fit an existing
power supply alongside a motor. Mean Well WDR-60-5 was chosen as a power
supply because it can achieve the desired output and the input voltage range is

very close to the voltage range of this project. In this option, when the voltage conversion circuit is prebuilt, the functionality of the WDR-60-5 needs to be studied when connected to the output of a frequency converter. The functionality will be examined by simulating the circuit of the power supply in normal operation and at the output voltage of a frequency converter, and by comparing their results. A take from the technical specifications of the selected power supply is shown in Table 1 and the block diagram of the device is shown in Figure 10. /10/

Table 1. Mean Well WDR-60-5 power supply technical data.

WDR-60-5		
Output	DC voltage	5 V
	Rated current	10 A
	Current range	0 – 10 A
	Rated power	50 W
	Voltage range	5 – 6 V
Input	Voltage range	180 – 550 Vac / 254 – 780 Vdc
	Frequency range	47 – 63 Hz
	Efficiency	83,5% / 400 Vac
	AC Current	0,4A/400 Vac | 0,7A/230 Vac
	Inrush current (max)	COLD START 50 A/400 Vac | 30 A/230 Vac
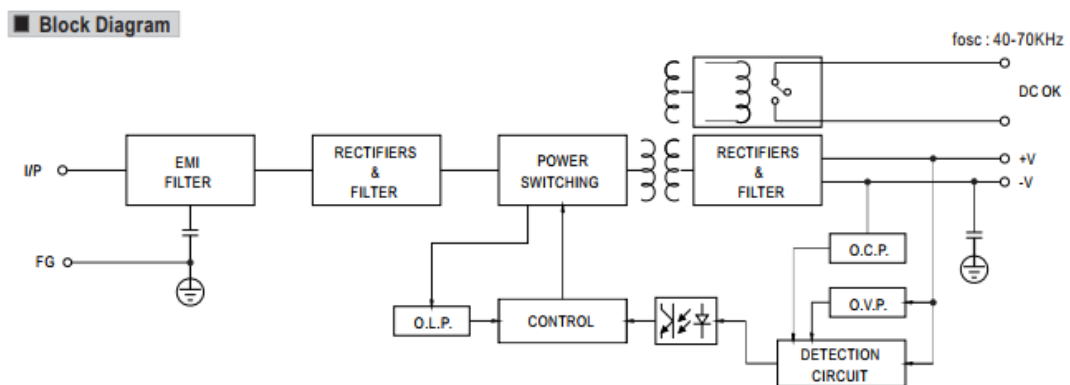
Figure 10. Mean Well WDR-60-5 power supply block diagram.

The suitability of the Mean Well WDR-60-5 power supply for frequency converter operation alongside a motor is simulated before the actual tests. The input circuit of the device, i.e. sections "EMI FILTER" and "RECTIFIERS & FILTER" indicated by

the block diagram, are examined in the simulations. This section is simulated at a normal sine voltage to obtain an idea of how the device is operating normally and with the PWM output provided by a frequency converter. The input circuit of the device has been determined by disassembling the device and examining the circuit board. A sketch of the input circuit and the circuit board is shown in Figure 11.
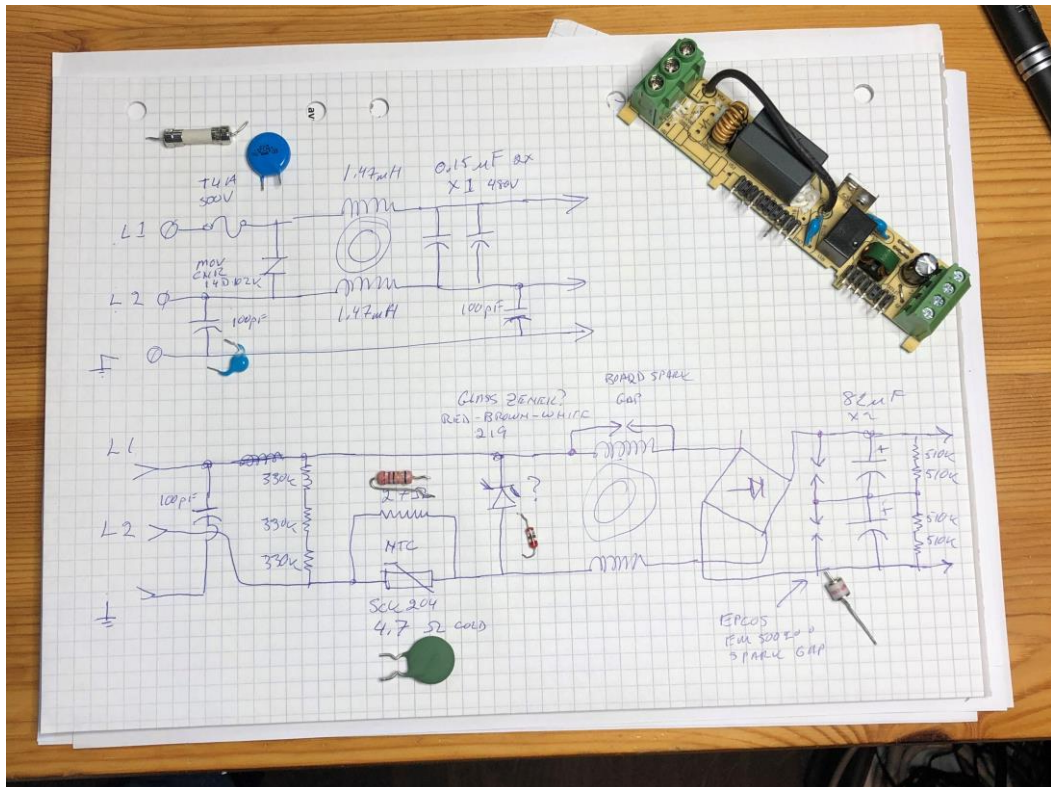
Figure 11. Input circuit diagram and the circuit board. /11/

4   SIMULATIONS

The PSCAD 5.0.0 software was used to simulate the electrical systems, for which a trial version of a student license was obtained for the duration of this project. PSCAD is a design tool for power systems developed by Manitoba Hydro, a Canadian company founded in 1961 /12/. The following paragraphs show the simulation models used in the project, their operation, and the results obtained.

4.1 Frequency Converter

The output of the frequency converter is simulated with three PWM voltage control modules controlled simultaneously with the same controllers. The controllers of the PWM modules control the output peak voltage, as well as the magnitude, frequency and phase angle of the reference sine wave to the switching logic. DTC signal has not been simulated separately. Figure 12 shows the frequency converter simulation model as phase voltage generation modules and their controllers.
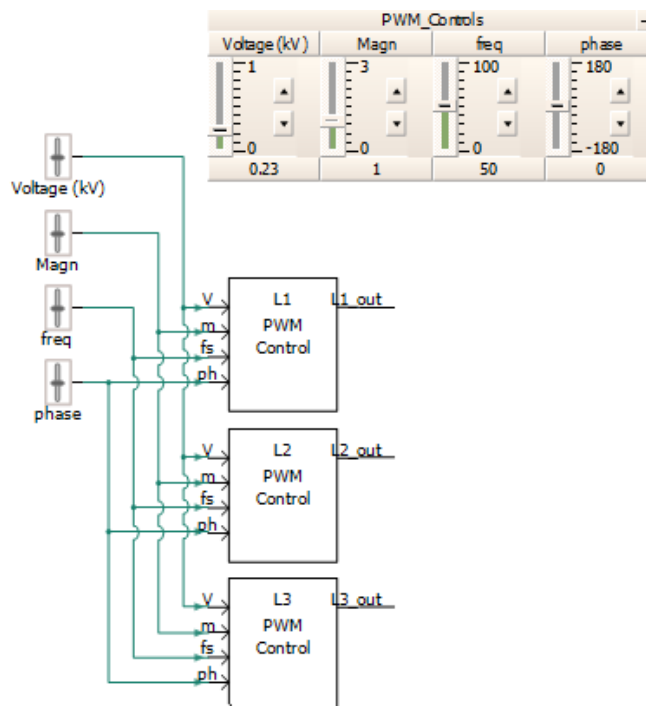
Figure 12. Frequency converter simulation model.

Phase voltage modules consist of a DC circuit and a switching logic controlling it, as shown in Figure 13. This simulation is repeated in each module with the difference that the reference sinewave of each module is at a phase angle of 120° to each other. The switching frequency and pulse width can be simulated with a triangular carrier wave of 4000 Hz, which is compared to the reference sine wave. The switching frequency was chosen to be 4000 Hz, as the waveforms of the signal remain relatively clear to view sufficiently long intervals at a time in the simulations. The logic portion of the modules control the transistors of the DC circuit so that the output provides negative voltage pulses when the value of the reference sine wave is lower than the carrier wave , and positive voltage pulses when the value of the reference sine wave is greater   than the carrier wave. In the example in Figure 13, the transistor G11 switches positive pulses and G12 switches negative pulses. Transistors are never both on at the same time, as the output voltage would then be 0V. Figure 14 shows the output voltage in 230 V pulses produced by this model compared a reference sine wave of the same amplitude and output current, as well as the 50 Hz reference sine wave used in the switching logic, 4000 Hz carrier wave and control signal of G11 transistor. The control signal of G12 transistor is G11 inverted.
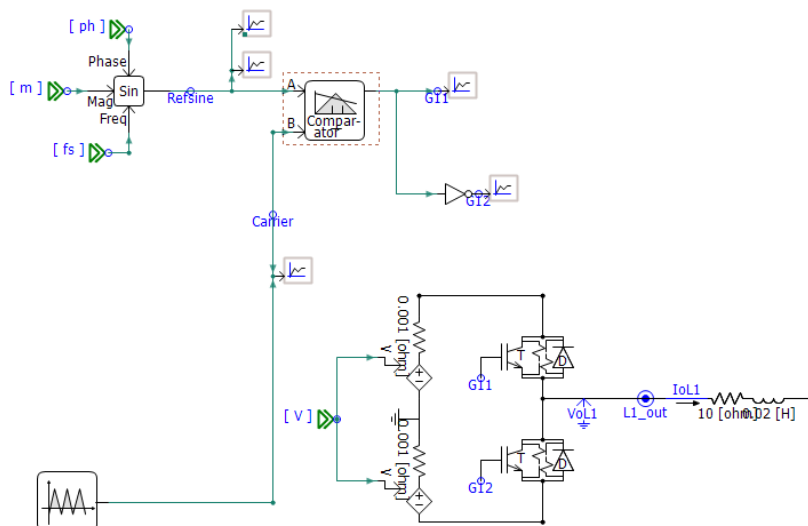
Figure 13. PWM voltage generation logic.
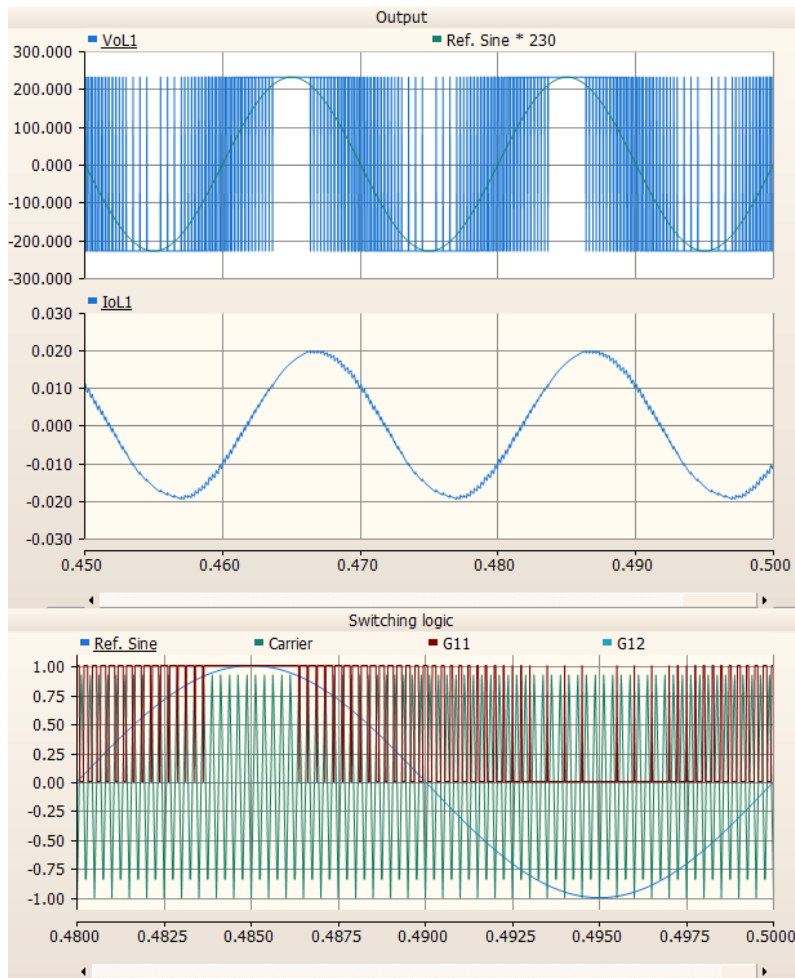
Figure 14. Waveforms of PWM generation logic and output.

4.2 NTC-thermistor

Inside the power supply, a SCK204R7 NTC thermistor is used in the filtering circuit to reduce the inrush current. The resistance of the NTC thermistor increases as temperature decreases. The effect of the NTC to inrush current in different temperatures and resistance values can be examined by simulating this. The following equation applies to the relation between NTC resistance values:

$$\frac{R1}{R2} = e^{\beta\left(\frac{1}{T1} - \frac{1}{T2}\right)} \tag{6}$$

Where R1 is the resistance in temperature T1,

R2 is the temperature in T2 and

β is temperature constant that is negative on a NTC thermistor.

Temperatures are indicated as Kelvins in the equations /13/. Equations 7 and 8 can be derived from Equation 6 for calculating the resistance of the NTC thermistor at a temperature specified in the simulation.

$$\beta = \frac{\ln\left(\frac{R2}{R1}\right)}{\frac{1}{T1} - \frac{1}{T2}} \tag{7}$$

Where the cold state (T1=25°C) resistance of NTC, 4.7 Ω, is used as R1. The resistance R2 of NTC at temperature T2 is selected from its datasheet, which in this case is about 5,7 Ω at temperature of 20 °C /14/. Equation 7 is used to calculate the temperature coefficient of the NTC, which is needed in Equation 8 for calculating resistance values at a given temperature.

$$R2 = R1 * e^{\beta\left(\frac{1}{T1} - \frac{1}{T2}\right)} \tag{8}$$

Where T2 is temperature in which the resistance is needed to be calculated. The calculated resistance R2 in the simulation is given to the variable resistance component in the circuit. With these calculations the resistance values for the NTC are between 110.2 Ω – 0.07 Ω on its operating temperature range of -40 °C – 200 °C. The resistance calculation logic in the simulation is shown in Figure 15.
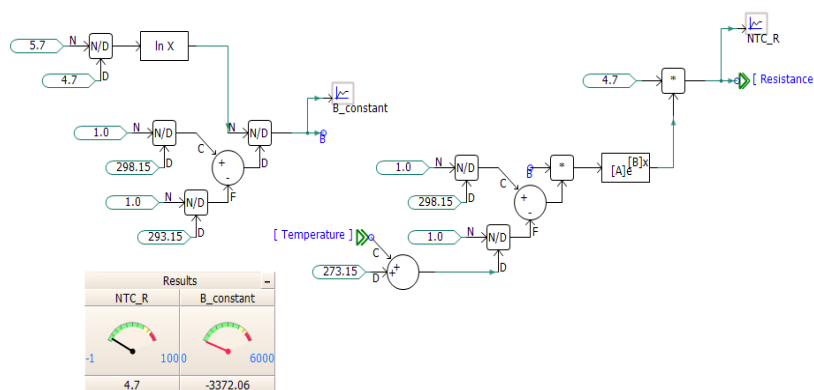
Figure 15. NTC thermistor calculation logic.

4.3 Motor

An induction machine with star connection supplied by a frequency converter is used in the simulations and tests. The motor is parametrized to correspond the ratings of the motor used in tests to ensure comparability of results. Figure 16 shows the motor in the simulation, as well as its controls and voltage measurements. Table 2 shows the parameters of the simulated motor.
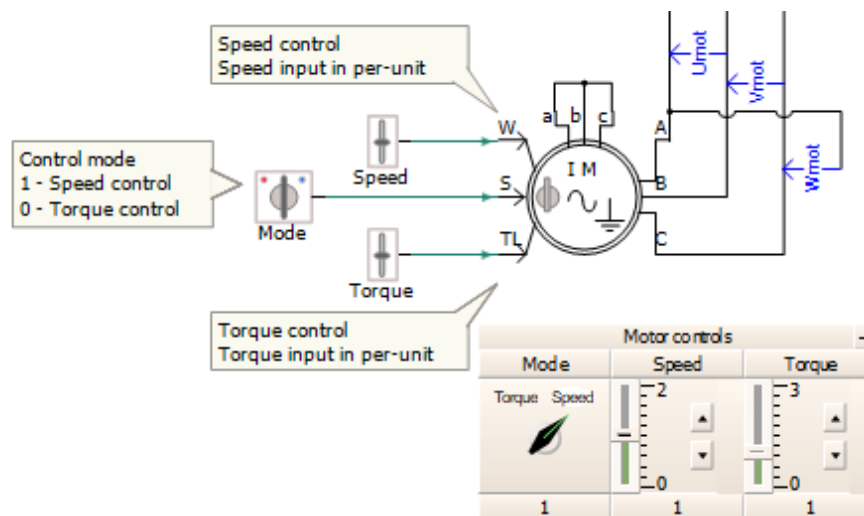
Figure 16. Electric motor used in the simulation.

Table 2. Parameters of the simulated motor.

Rated power	11 kVA
Voltage	690 V
Connection	Y
Angular frequency	307.67 rad/s

4.4 Simulation model of the power supply

The power supply input circuit is simulated as shown in Figure 17. The figure shows the measuring points for currents taken by the device I1 and I2, main voltage U12, bus voltages U1e and U2e, and DC side voltage Udc and current Idc. In addition, there is a 4 A glass pipe fuse in the actual device at the I1 measuring point. The circuit has been closed by connecting a 3300 Ω resistor as load for the examination

of this section. The resistance has been selected in such way that at the end of the rectifier the power will be almost the same as in normal operation at the output of the power supply.
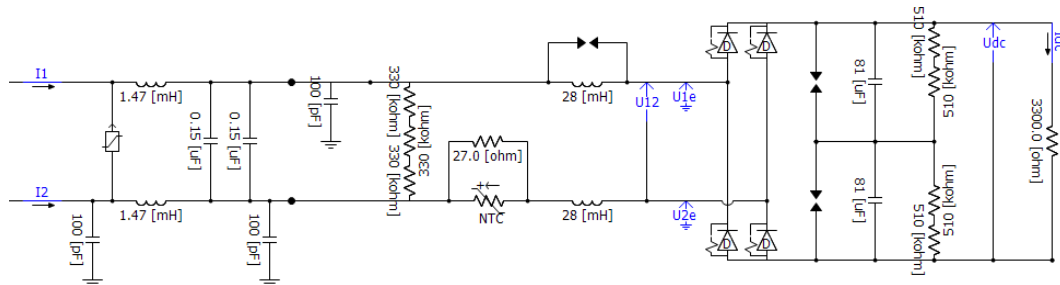
Figure 17. WDR-60-5 input circuit simulation model.

4.5 WDR-60-5 Fed with Sine Voltage

A simulation image of the power supply fed with mains voltage of 400 V sine wave is shown in (APPENDIX 1). The image shows the behavior of voltages and currents in normal operating mode. The following observations can be made:

1. When starting, the device will take a power surge of approximately 5 ms with a peak value of 12.21 A. After this the RMS value of the current will be at a level of approximately 0.85 A. The power surge taken by the device is caused from the capacitors in the filtering circuit charging up, during which the current of the circuit can rise higher than when the current levels out. This is shown in more detail in Figure 18.

2. On the DC side, a peak of approximately 74 ms (a) with peak values of 891.1 V and 270 mA (b) is generated at voltage and current. The voltage and current then level out to approximately 533 V and 162 mA. The voltage and current ripples are 29.8 Vp-p and 9 mAp-p (c). This is shown in more detail in Figure 19.
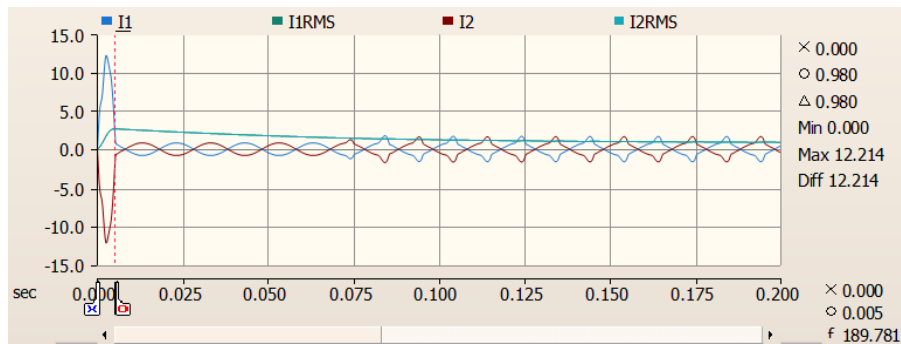
Figure 18. Current taken by the power supply in normal operation.
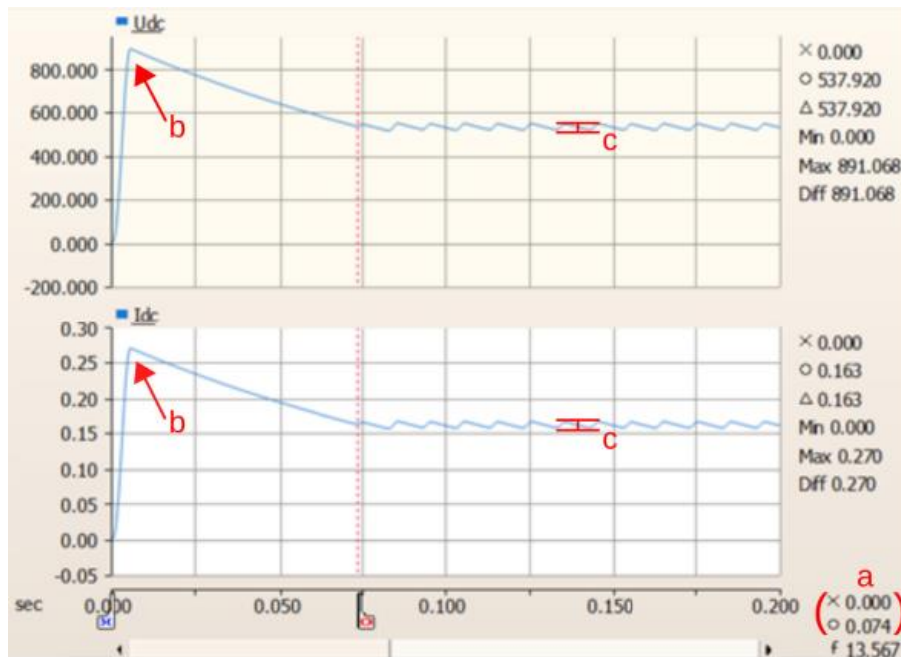
Figure 19. Voltage and current of input circuit's DC side in normal operating mode.

4.6 WDR-60-5 Fed with Frequency Converter

The simulation image of the power supply fed with a frequency converter is shown in (APPENDIX 2). The image shows the behavior of voltages and currents with PWM signal. The following observations can be made:

1. When starting, the device will take a power surge of approximately 5 ms with a peak value of 12.63 A. After this the RMS value of the current will

be at a level of approximately 2.45 A. The waveform of the current remains very spiky. The spikiness is due to the switching frequency of PWM signal, which is much higher than the frequency for which the filtering circuit is rated. After the starting current, the maximum instantaneous current values are 6.9A spikes of approximately 0.16 ms. This is shown in more detail in Figure 20.

2. On the DC side, a peak of approximately 110 ms is generated at voltage and current with peak values of 666. 2Vand 202 mA. The voltage and current then level out to approximately 405 V and 122mA. The voltage and current ripples are 10.0 Vp-p and 3 mAp-p. This is shown in more detail in Figure 21.
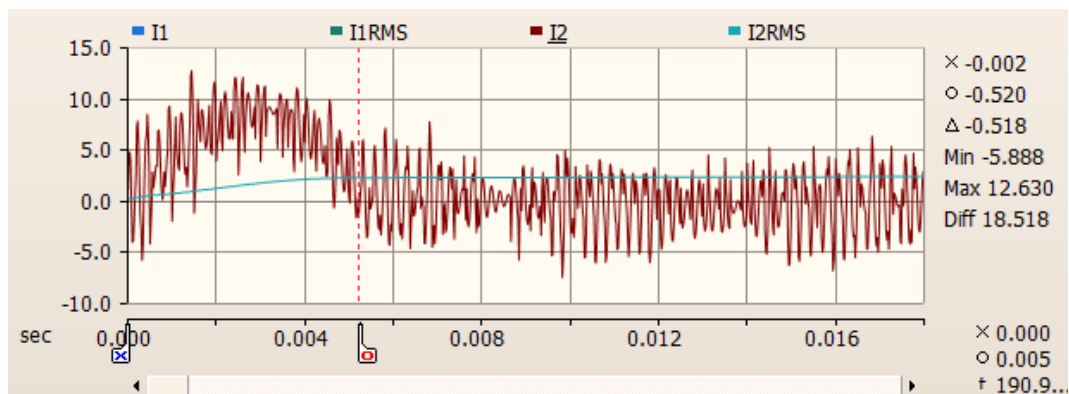
Figure 20. Current taken by the power supply when fed with a frequency converter.
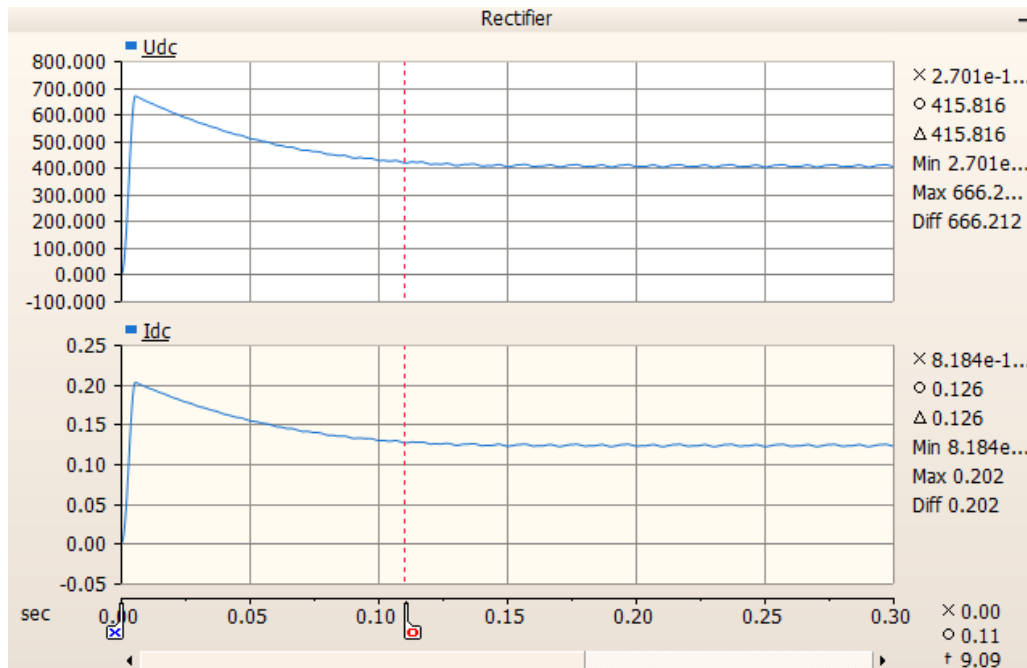
Figure 21. Voltage and current on the DC side of the input circuit when fed with a frequency converter.

The results show that compared to the normal operating situation, the starting current taken by the device is not much higher, but after that the current is almost three times higher with the PWM feed. In both cases, the power surge in the start-up situation is equally long. On the DC side, the start-up spike takes more time to level off with PWM input than in normal operation with sine voltage. The voltages and currents on the DC side are slightly lower with the PWM feed than in normal operating conditions. The problem with feeding WDR-60-5 with a frequency converter is the high input current it takes on startup, which trigger the safety functions on smaller frequency converters. For this reason, the device can only be tested in its original state with larger drives that can also supply the starting current taken by the device. This issue should be resolved when developing the project. The results of these operating situations and a comparison are compiled in Table 3.

Table 3. Results and comparison of the normal operating situation and the PWM-fed situation.

		Normal operation	PWM feed	Alteration
Input current	Inrush current duration	5 ms	5 ms	±0 ms
	Inrush current peak	12.21 A	12.63 A	+0.42 A
	Levelled current (RMS)	0.85 A	2.45 A	+1.6 A
DC side	Start-up surge duration	74 ms	110 ms	+36 ms
	Voltage peak	891.1 V	666.2 V	-224.9 V
	Levelled voltage	533 V	405 V	-128 V
	Voltage ripple	29.8 Vp-p	10 Vp-p	-19.8 Vp-p
	Current peak	270 mA	202 mA	-68 mA
	Levelled current	162 mA	122 mA	-40 mA
	Current ripple	9 mAp-p	3 mAp-p	-6 mAp-p

4.7 WDR-60-5 in Parallel with a Motor

A simulation image of the power supply, fed with a frequency converter, in parallel with a motor, is shown in Appendix 3. The image shows the behavior of voltages and currents with a PWM signal when the device is connected in parallel with a motor. The following observations can be made:

1. When starting, the device will take a power surge of approximately 5 ms with a peak value of 12.62A. After this the RMS value of the current will be at a level of approximately 2.45 A. The waveform of the current remains very spiky. After the start current, the maximum instantaneous current values are 6.7 A spikes of approximately 0.16 ms. The results are almost the same as without a motor in parallel with the power supply.

2. On the DC side, a peak of approximately 110 ms with peak values of 665.9 V and 202mA is generated at voltage and current. The voltage and current then level out to approximately 403 V and 123 mA. The voltage and current ripples are 10.1 Vp-p and 3 mAp-p. The results are almost the same as without a side-by-side engine.

In this simulation, the effect of motor cable to the measurements is also examined by adding RLC-components between the frequency converter and motor. The values of these components have been estimated amounts for a 10-meter cable. The motor cable is simulated as shown in Figure 22. In the simulation model, the resistance of the conductor is 87,7 mΩ, inductance is 0,35 mΩ and the capacitance between conductors are 1 pF. These values are based on the estimated impedances for 4x2.5 size copper cables shown in the table of Figure 23. As an effect of the motor cable on the measurements in the power supply, the following changes are noted:

1. The device will now take a 12.03 A power surge at startup. The RMS current value then levels at 2,69 A. After the start-up current, the maximum instantaneous current values are about 7.7 A.

2. On the DC side, a peak of approximately 150 ms is generated at voltage and current with peak values of 661.3 V and 200mA. The voltage and current will then level at approximately 423 V and 128mA. The voltage and current ripples are 8.4 Vp-p and 3mAp-p. This is shown in more detail in Figure 24.
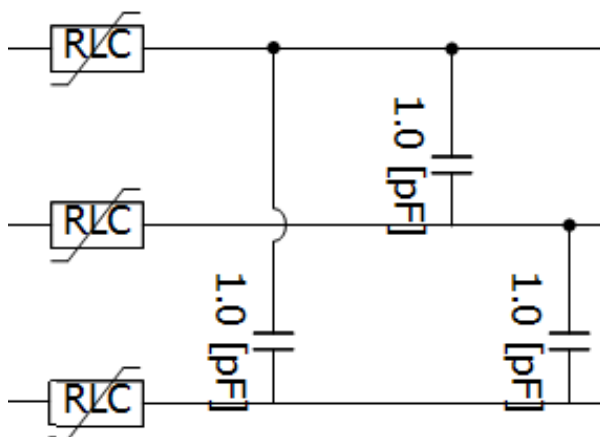

Figure 22. Simulation model for the motor cable.

Johtimien poikkipinta A/mm²	Kupari			Alumiini		
	Resistanssi r	Reaktanssi x	Impedanssi z	Resistanssi r	Reaktanssi x	Impedanssi z
4 × 1,5	14,620	0,115	14,620			
4 × 2,5	8,770	0,110	8,770			
4 × 4	5,480	0,107	5,480			
4 × 6	3,660	0,100	3,660			
4 × 10	2,244	0,094	2,246			
4 × 16	1,415	0,090	1,418	2,324	0,090	2,326
4 × 25	0,898	0,086	0,902	1,489	0,086	1,492
4 × 35	0,652	0,083	0,657	1,086	0,083	1,089
4 × 50	0,482	0,083	0,489	0,796	0,083	0,800
4 × 70	0,336	0,082	0,346	0,551	0,082	0,557
4 × 95	0,244	0,082	0,257	0,398	0,082	0,406
4 × 120	0,195	0,080	0,211	0,316	0,080	0,326
4 × 150	0,155	0,080	0,174	0,258	0,080	0,270
4 × 185	0,125	0,080	0,148	0,207	0,080	0,222
4 × 240	0,095	0,079	0,124	0,162	0,079	0,180
4 × 300	0,078	0,079	0,111	0,133	0,079	0,155

Figure 23. Approximate impedances of cables at conductor temperature 80 °C (Ω/km). /15/
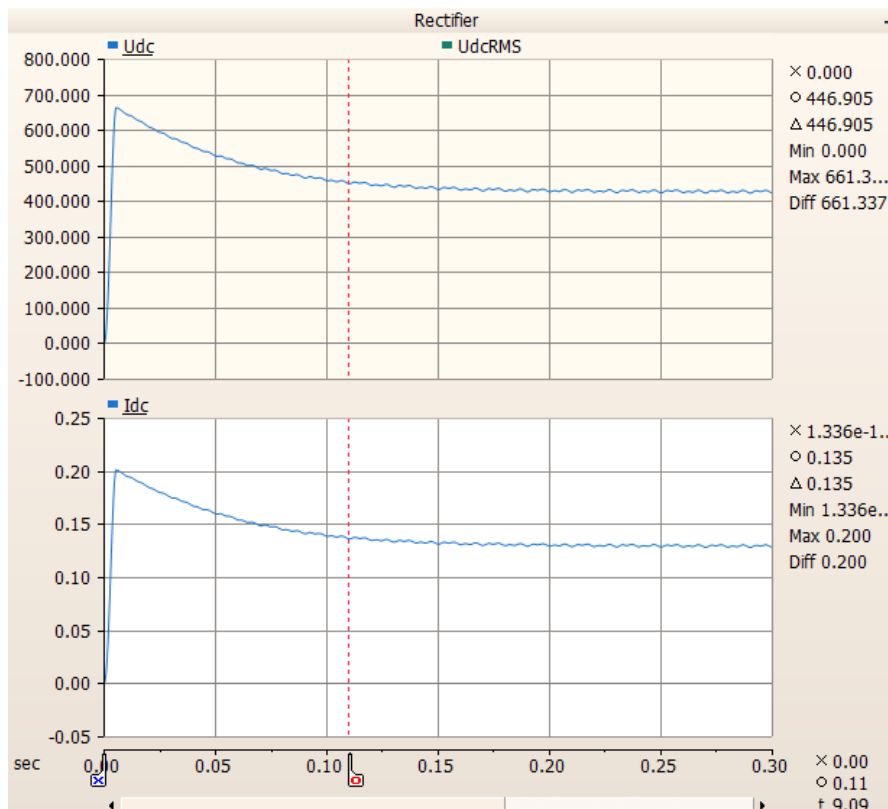
Figure 24. Voltage and current on the DC side of the input circuit when fed with a frequency converter, in parallel with a motor and simulated motor cable.

The results show that the addition of a motor to the simulation in parallel with the power supply has little effect on the values measured in the power supply. The simulation of a motor cable, on the other hand, generates minor changes in the results. Among other things, the addition of the motor cable will reduce the starting current taken by the device, which is expected, as new impedances will appear in front of the device. For the same reason, on the DC side, the start-up spikes are slightly smaller than without a simulated engine cable. The capacitance between conductors, on the other hand, extends the leveling time of the start-up spikes on the DC side. Table 4 summarizes the results of measurements of the power supply fed with PWM voltage connected in parallel with a motor with and without the simulated motor cable, as well as a comparison between these cases.

Table 4. Measurement from the power supply fed with PWM voltage, in parallel with a motor, with and without a simulated motor cable.

		Without motor cable	With motor cable	Alteration
Input Current	Inrush current duration	5 ms	5 ms	±0 ms
	Inrush current peak value	12.62 A	12.03 A	-0.59 A
	RMS current	2.45 A	2.69 A	+0.24 A
DC side	Start-up surge duration	110 ms	150 ms	+40 ms
	Voltage peak	665.9 V	661.3 V	-4.6 V
	Levelled voltage	403 V	423 V	+20 V
	Voltage ripple	10.1 Vp-p	8.4 Vp-p	-1.7 Vp-p
	Current peak	202 mA	200 mA	-2 mA
	Levelled current	123 mA	128 mA	-5 mA
	Current ripple	3 mAp-p	3 mAp-p	±0 mAp-p

5   TESTING

During the testing phase, the simulation-based connections were made at the test field of the ABB motors plant in Vaasa, and the operation of the device was examined. Two power supplies were used in the tests, one of which was in the original condition and the other one had conductors brought out from the input circuits rectifier. The latter was intended to be used to ensure the accuracy of simulation results from the DC side. The frequency converter used in the tests was ABB ACS880-01 (29kVA), which supplied a star connected motor with scalar control. Technical data of the frequency converter is shown in table 5 and an image of the frequency converter in Figure 25.

Table 5. Technical data of the frequency converter used in the tests.

		ABB ACS880
	Pn	18.5 kW
Input	U1	400 V
	I1	34 A
	f1	50 / 60 Hz
Output	U2	3~ 0…U1
	I2	34 A
	f2	0-500 Hz

Figure 25. ABB ACS880-01 -frequency converter.

In the first test, the normal operation of the device was ensured by plugging it into a standard single-phase socket. The power supply was then tested with a frequency converter fed in parallel with a motor. When fed with a drive, fuses were added in front of the power supply to protect the internal fuse of the device. A 3300 Ω resistor was connected to the output of the power supply, over which voltage was measured. The connections between the frequency converter and the motor are shown in Figure 26, and the connection of the power supply in the first test with a frequency converter is shown in Figure 27.
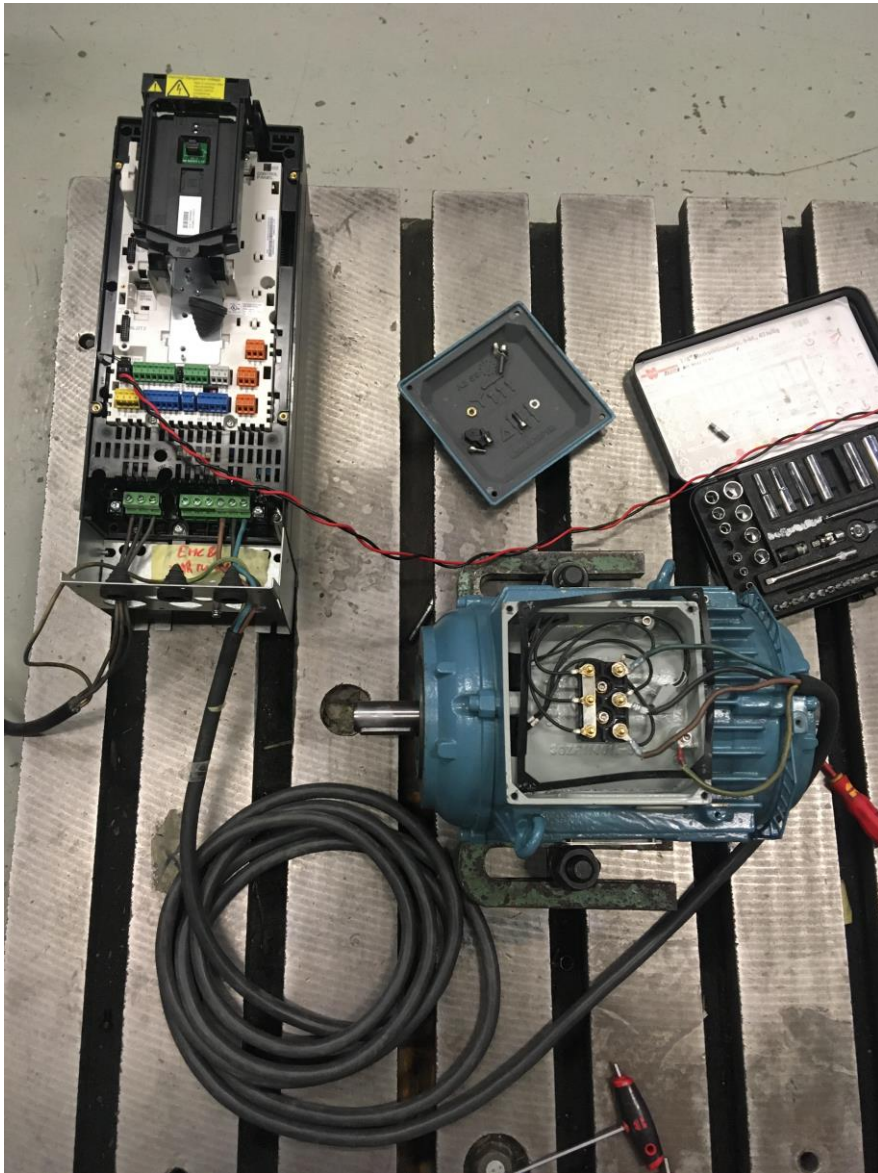
Figure 26. Connection of the frequency converter and the motor.

Figure 27. Connection of the power supply in the first test with a frequency converter.

In this test, an automatic fuse was used in front of the power supply. The internal fuse burned immediately, and smoke started rising from the automatic fuse. The most likely reason for the automatic fuse to burn is that it was selected according to the constant values of the current taken by the device, without taking more account of the peak values. In normal operation, the maximum peak values of the current taken by the device are approximately 1.6 A, while with frequency converter signal it is 7.7 A, but much shorter in duration. The fuse was then replaced

on the power supply, as well as the automatic fuse was replaced with a motor starter, on the assumption that it would withstand the frequency converter signal better. As a result of the test, the device gave a 5 V output for approximately three seconds before the motor starter tripped. This is probably due to the same reason why the automatic fuse did not work either, although in this case the motor starter handled the PWM voltage better than the automatic fuse.

In the final tests, the power supply was fed directly by the frequency converter, using ceramic 4 A fuses for both supply cables in front of the power supply. The power supply with leads brought out from the inputs DC side for examination of measurements was used in this test. The measurements taken with an oscillo-scope from this test are the input current to the power supply (see I1 in the simu-lation model figures) and DC side voltage (Udc in simulation model). The test con-figuration without the oscilloscope probes is shown in Figure 28.
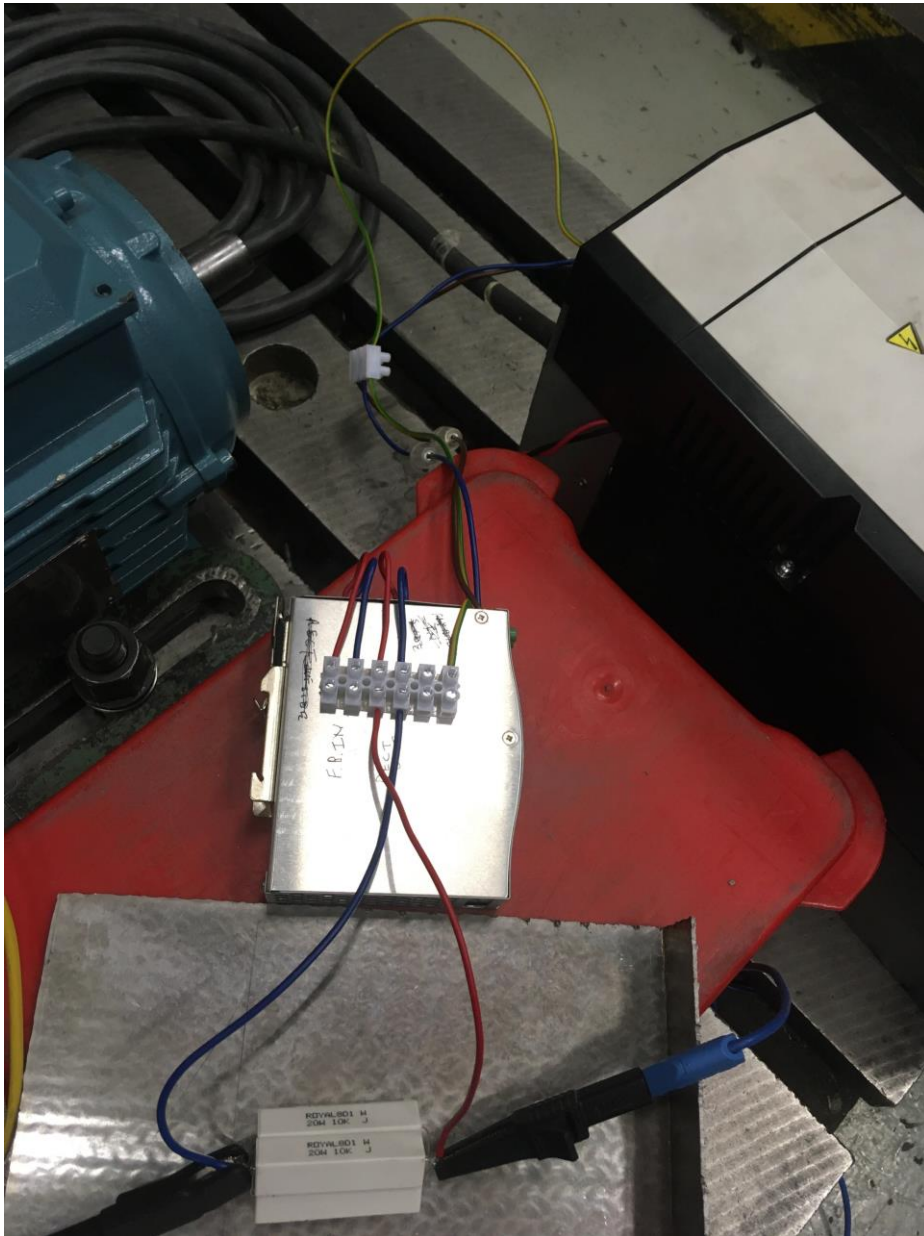
Figure 28. Testing configuration of the modified power supply (testing of the DC side of the input circuit. Connection corresponding to the simulation model).

In the figure, the wiring of the connection strip is made so that the DC side of the input circuit can be examined as shown. To reconnect the input circuit with the rest of the circuit in the device, the wires would be connected to the adjacent connectors of same wire coloring. Tests on the DC side showed voltage of 534 V at start-up on a multimeter before an external fuse burned. In tests of the entire

device with external ceramic fuses, the device gave 5 V on its output, again for a very short time, and then burned the external fuse.

An explanation can be sought here for the burning of the external fuse in the data sheets of the fuses used. Figure 29 shows a table of the melting times reported by the fuse manufacturer at different odds of the rated current. Based on the results provided by the simulation, a 5 ms-long 12 A current surge should not yet burn the fuse, but subsequent surges may have caused this over time. According to the simulation results, the peak current values after the start-up current peak are set between the rated current odds of 1,5 and 2.

I_N - t Verhalten / I_N - t characteristics:

Bemessungs-strom-Faktor / Rated current factor		Schmelzzeit / Melting time:	
		100 mA – 25 A	20 A – 25 A
1,15 · I_N	t_{min}	60 min	
	t_{max}	-	
1,5 · I_N	t_{min}	0	
	t_{max}	30 min	
2 · I_N	t_{min}	0	
	t_{max}	3 s	
10 · I_N	t_{min}	0	
	t_{max}	15 ms	

Figure 29. Melting times of external fuses used in the tests. /16/

6   ANALYSIS

In this chapter, the oscilloscope measurements are examined and compared to the simulation results. The measurements are also used to justify the behavior of the actual device during the tests. Teledyne Lecroy HDO6054 oscilloscope was used in the tests.

6.1 Results with Scalar Control

The oscilloscope images show the current taken by the WDR-60-5 (yellow, I1, C1) and the DC side voltage of the input circuit (red, Udc, C2). Figure 30 shows these measurements over a 500 ms period.
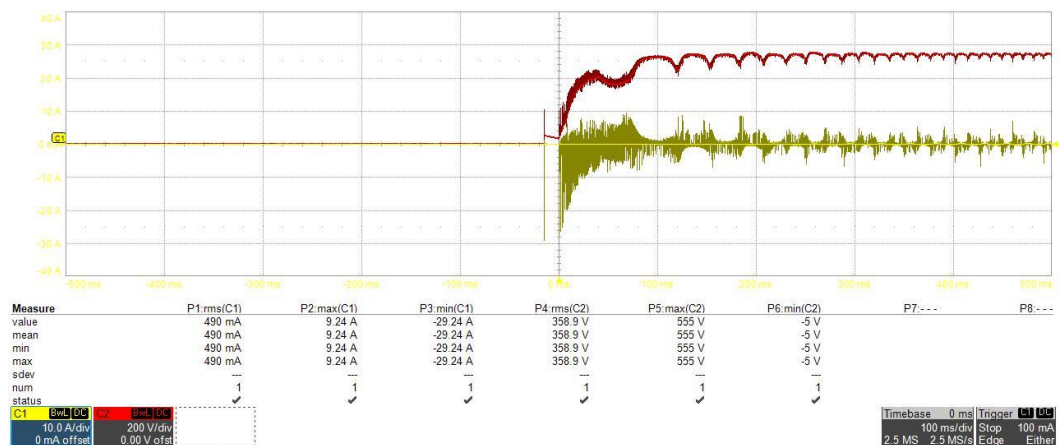
Figure 30. Input current (yellow, C1) and DC side voltage (red, C2) of WDR-60-5 fed with scalar control over 500 ms period.

In Figure 30, the time division is 100 ms, voltage division is 200 V and current division is 10 A. A switching frequency of 4500 Hz was used during the tests, and ramping time was set to 0.5 s. This results in the long form of the first voltage cycle, as well as the gradual reduction in the shape. Compared to the simulation, this measurement lacks the surge in the voltage at startup. This is probably because the simulation does not take the acceleration ramp into account but feeds the circuit immediately with full signal. In the measurements, the voltage levels out at about 555 V, which is approximately 130 V higher than the simulated result, but in the

same order of magnitude as in the normal operating situation. On this basis, it can be concluded that the voltage is in order at this point in the circuit.

The current taken by the power supply has been measured in relation to the simulation image at the I1 measuring point. It is taken into account that the current values presented in the thesis are of I2, which according to the simulation is almost the same as I1 inverted. According to this measurement, the maximum value of the inrush current is approximately 29.2A, which is more than double the inrush current from the simulation. This explains why smaller frequency converters tripped in other tests right at startup. Towards the end of the time period, a more leveled waveform is seen, which is again found to be spiky as in the simulation. The waveform and biggest spikes of the leveled current appear to be very close to the results of the simulation.

6.2 DTC Results

The same measurements were repeated using DTC control. Figure 31 shows the input current to the power supply fed with DTC and the DC side voltage of the input circuit in the same way as in the previous paragraph. The time division in this case is 20 ms.
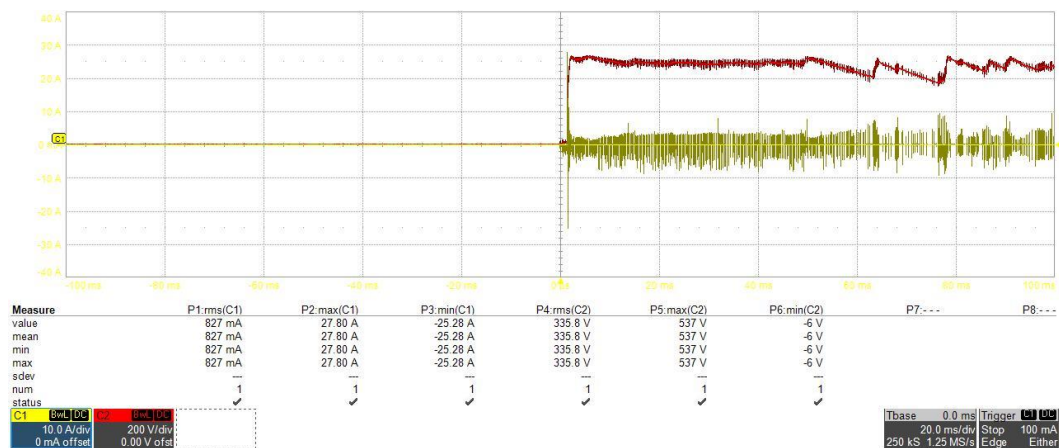
Measure	P1:rms(C1)	P2:max(C1)	P3:min(C1)	P4:rms(C2)	P5:max(C2)	P6:min(C2)	P7:- - -	P8:- - -
value	827 mA	27.80 A	-25.28 A	335.8 V	537 V	-6 V		
mean	827 mA	27.80 A	-25.28 A	335.8 V	537 V	-6 V		
min	827 mA	27.80 A	-25.28 A	335.8 V	537 V	-6 V		
max	827 mA	27.80 A	-25.28 A	335.8 V	537 V	-6 V		
sdev	---	---	---	---	---	---		
num	1	1	1	1	1	1		
status	✓	✓	✓	✓	✓	✓		

Figure 31. Input current (yellow, C1) and the DC side voltage (red, C2) of WDR-60-5 fed with DTC over a 100 ms period.

With DTC, the DC side voltage rises much faster to its operating value, where it remains fairly steadily. The voltage changes detected towards the end of the time period are probably due to changes in the active switching combination when accelerating the engine. The ramping time in this case as well is 0.5 s. The DC side voltage differs from the simulated results with the PWM voltage again but is very close to the voltage levels of the normal operating situation and the results from scalar control. On this basis, it can be concluded that the voltage is in order at this point in the circuit.

The current taken by the power supply levels out much faster with DTC than with scalar control. At the very beginning, short inrush current spikes of about 27,8 A can be seen, but these level out to the steady state quickly. For the most part the current in steady state remain less than 5 A, but the maximum peaks are almost 10 A. Figure 32 shows the starting current taken by WDR-60-5 fed with DTC, revised to the first pulses. The time division is 200 µs. This shows that with DTC and a short ramping time, WDR-60-5 takes huge inrush currents for only two 120 µs pulses. According to this measurement, the peak current value is about 31.1 A, and the peak of the second pulse is about 15 A.
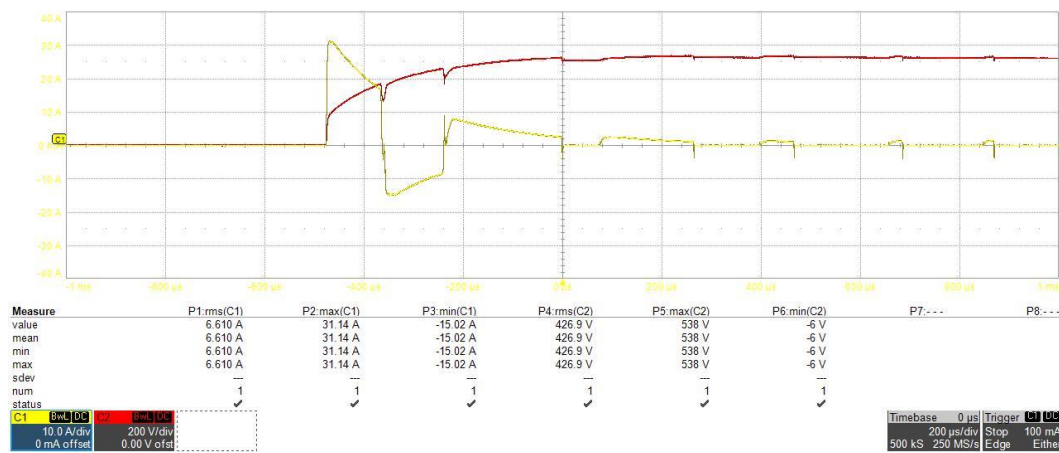
Figure 32. Input current (yellow, C1) and the DC side voltage (red, C2) of WDR-60-5 fed with DTC over a 1 ms period.

6.3 Conclusions

Measurements show that with both controls, the DC side voltage of the input circuit levels out at the same values as in the normal operating situation. This suggests that in favor of voltage, the WDR-60-5 could operate in a frequency converter application. The assumption is that if at this point the signal looks the same with the frequency converter input as in the normal operating situation, the power supply should work appropriately when reconnecting this section to the rest of the circuit.

In the current state, WDR-60-5 problems as a 5 V power supply connected to a motor are the high inrush currents it takes. Especially due to the 30 A inrush current spikes seen here, there is no possibility of using this power source in smaller frequency converters in its original state. However, in addition to tripping the frequency converters, these currents also burn the internal fuse of WDR-60-5. In order to make the WDR-60-5 function as a 5 V output suitable for all motors, its input circuit would have to be redesigned to take less current with a high-frequency feed. This topic is reviewed more in development ideas.

7 DEVELOPMENT IDEAS

This chapter reviews options for continuing and developing the project. The ideas are either about modifying the power source used here, or about studying and testing an alternative power source. Modifying the power supply would probably require cooperation with the manufacturer of the device, where the manufacturer would be asked to make the device with a new input circuit, after which this could be ordered and retested. In case of an alternative power supply, similar simulations and tests should be repeated with the other device.

7.1 Redesigning the filtering circuit for high frequencies

In order to make the studied power supply work with the input of a frequency converter, its filtering circuit would need to be redesigned for high frequencies. The examination of the device was initiated on the assumption that it could be fed with a frequency converter when its output simulates a 50 Hz sine-shaped voltage. However, after the tests, it was found that rather than the reference frequency, the input frequency to the power supply must be considered according to the switching frequency, that is typically about 1 kHz – 16 kHz depending on the frequency converter. When redesigning the input circuit, capacitors give the greatest impact on the results. The change in the resistance value of the NTC thermistor was also found to reduce the start-up current quite well.

As an example case, the power supply input circuit model was modified where the 0.15 µF capacitors between buses were removed and the original 81 µF capacitors after the rectifier were replaced with 22 µF capacitors. These changes are estimates of the values for the components to make the device work better when supplied with a frequency converter. More detailed values for the input circuit and any changes in the structure must be examined separately. The simulation model of the modified power supply is shown in Figure 33. When simulating this at PWM voltage, the following differences from the original device are noticed:

1. The inrush current taken by the device is now only 4.5 A, which lasts for 3 ms. The steady-state current is now much more leveled and does not have very high surges. The steady-state current has the RMS value of 0.65 A and the highest surges are 1.4 A. The steady-state current is very close to the input current in the normal operating situation and small enough not to burn the internal fuse. These are shown in Figure 34.

2. The voltage and current surges on the DC side on start-up are much shorter and smaller, but the ripple is larger. These are shown in Figure 35.
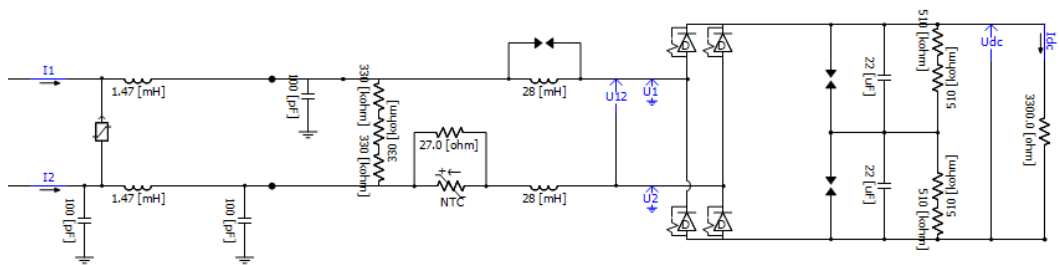
Figure 33. Simulation model of the modified power supply.
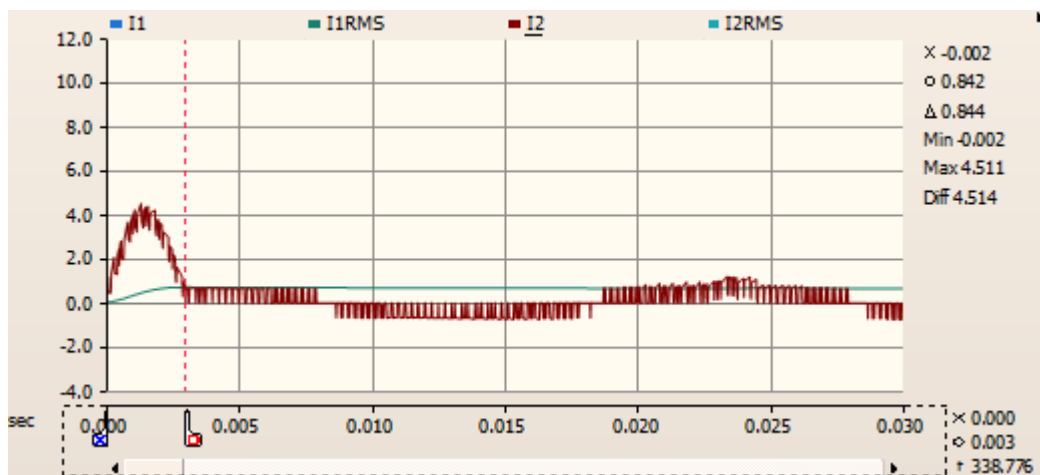
Figure 34. Input current to the modified power supply when fed with a frequency converter.
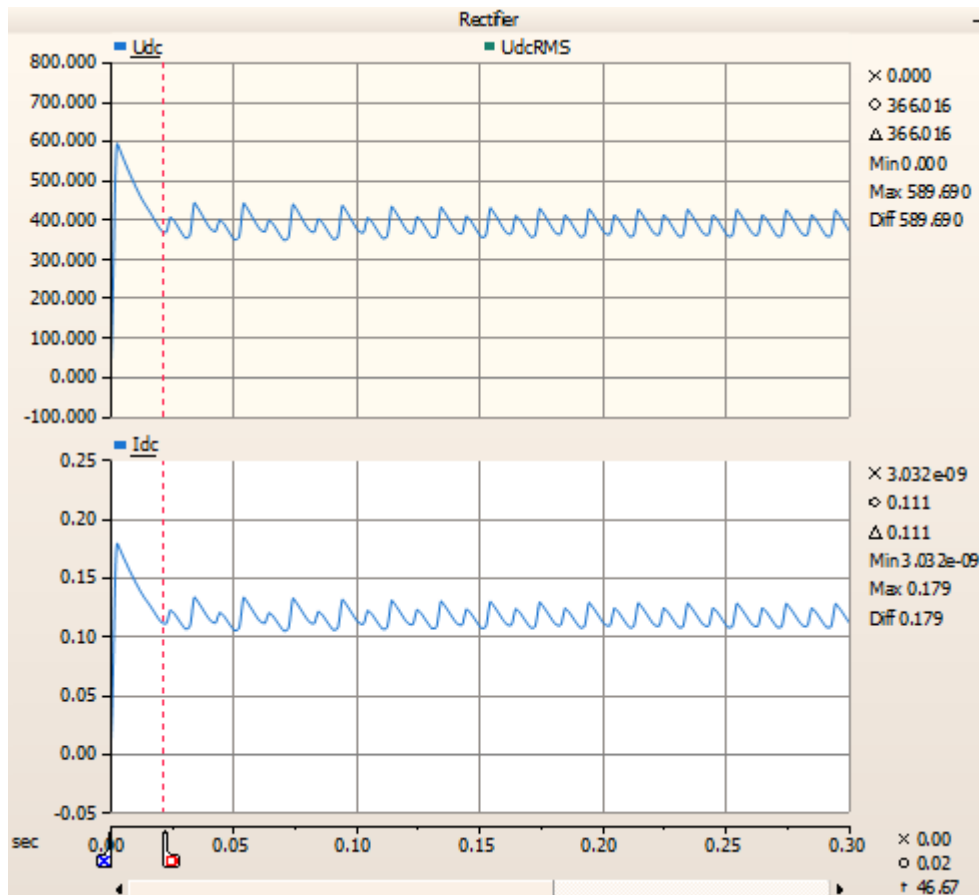
Figure 35. Voltage and current in the DC side of the input circuit on the modified power supply when fed with a frequency converter.

The current taken by the power supply is very close to the input current of the normal operating situation and within the limits of the internal fuse. The above changes were made to one of the power supplies used in the tests, after which the device seemed to work a little better when fed with a frequency converter. In the tests for the modified power supply, ABB ACS880-01 (2.2 kW), and Vacon NXS (2.2 kW) frequency converters tripped immediately but works and provides a steady 5 V DC output with ACS225 (1.5 kW). The technical data of these frequency converters are given in table 6.

Table 6. Technical data for the frequency converters used in the tests for the modified power supply.

		ABB ACS225	ABB ACS880	Vacon NXS
	Pn	1,5 kW	2,2 kW	2,2 kW
Input	U1	1~ 200-240 V	3~ 400 V	3~ 380-500 V
	I1	12,9 A	5,6 A	5,6 A
	f1	48…62 Hz	50 / 60 Hz	45…66 Hz
Output	U2	3~ 0-250 V	3~ 0…U1	3~ 0-U1
	I2	7,0 A	4.8 A	4.3 A
	f2	0-500 Hz	0-500 Hz	0-320 Hz

Figure 36. ABB ACS255 frequency converter.

7.2 Modifying the Input to be Three-Phased

This can be thought of as the next development step for what was presented in the previous paragraph. Converting the power supply to three phases instead of a two-phase solution would help offset the load on the frequency converter. This requires yet another dimensioning for the filtering circuit and the new, third bus.

This solution was not tested in practice during the thesis because the changes are too big to be made on the original circuit boards and fit into the original enclosure of the device. The three phased power supply would be similar to that shown in Figure 37.

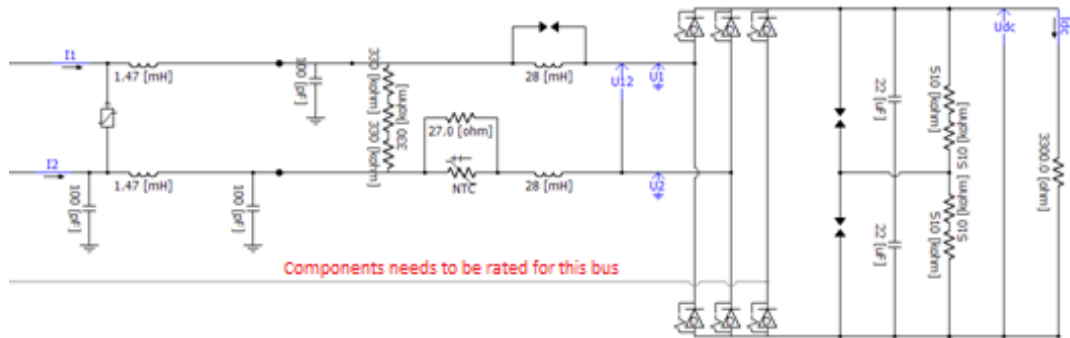**Figure 37.** Example of a three phased modified input circuit.

7.3 Use of Another Power Supply

Optionally, an alternative power supply could be used instead of Mean Well WDR-60-5. One option for this could be a power supply implemented with a LT8316 isolated flyback converter. Figure 38 shows one connection to this controller, which allows the controller to have a wide input voltage range of 20 to 800 V.
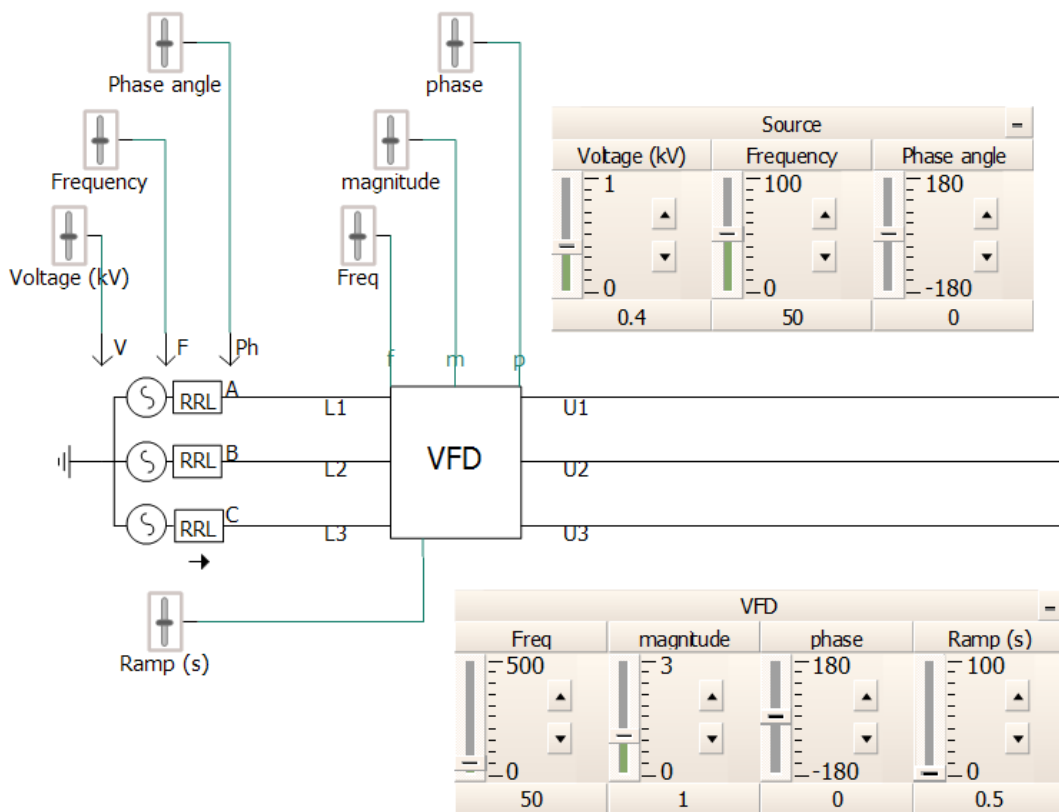
Figure 38. Connection diagram for the LT8316 based power supply /17/

The first step in the investigation of this option should be to see if this can be made to work with PWM input. The possibility of simulating these circuits depends on whether this controller is modelled and available in PSCAD. Also, the output transformer should be replaced with a smaller one, as the connection diagram shows a 12 V DC output.

7.4 Improving the Frequency Converter Simulation Model

The frequency converter model used in the thesis does not fully reflect the realistic output of a frequency converter but could rather be thought of as a very theoretical PWM generator. The output signal of an actual frequency converter is not quite as clean as the signal presented here, nor does this have other drive settings taken into account such as acceleration ramp. For the upcoming simulations, it would be useful to build a new frequency converter model that also takes into account other features used in a frequency converter. This paragraph presents a draft of a new simulation model for a more realistic frequency converter.

Figure 39. The new frequency converter simulation module and its supply.

The new simulation model for the frequency converter is built according to an actual frequency converter circuit. The connection diagram is shown in Figure 40. The frequency converter is fed with a three phase source, which is which is rectified on a 6-pulse rectifier. In the simulation, the DC intermediate circuit is open at baseline for half a second, after which the timed switches close and start the output. This allows the DC intermediate circuits capacitor to charge before connecting the output. After the DC intermediate circuit, the circuit has an IGBT connection that creates the PWM voltage, as well as the module for switching logic that controls it. In this version, the switching logic is practically the same as in the previous model with the differences that now the switching logics for each phase are on one page and an acceleration ramp has been added to the reference frequency. The new switching logic is shown in Appendix 4.
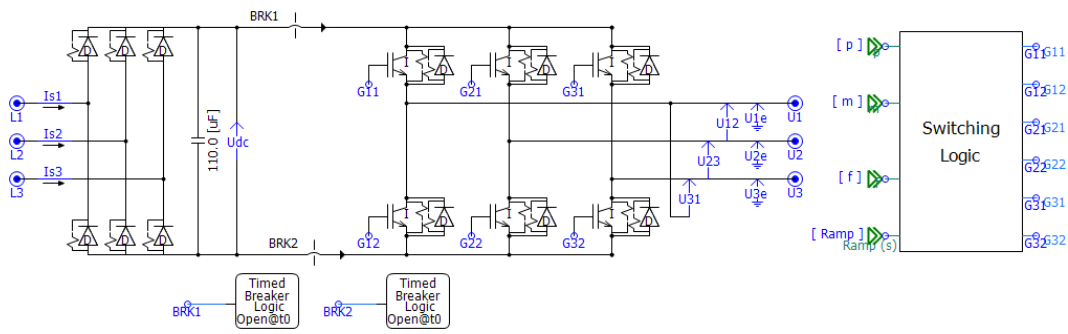
Figure 40. New frequency converter simulation model.

The acceleration ramp has been implemented in this simulation as shown in Figure 41. The ramp starts at the same time as the timed breakers in the circuit close (a) and acts as a multiplier between values of 0 and 1 for the reference frequency. A linear acceleration ramp is simulated by giving triangular wave a frequency at which it reaches the first quarter of its cycle (positive peak value) within the ramping time (b). The logic then waits until the triangular wave gets close enough to its peak value (c) to lock the reference frequency multiplier to 1 (d). This provides a triangular wave and the reference frequency multiplier as shown in Figure 42.
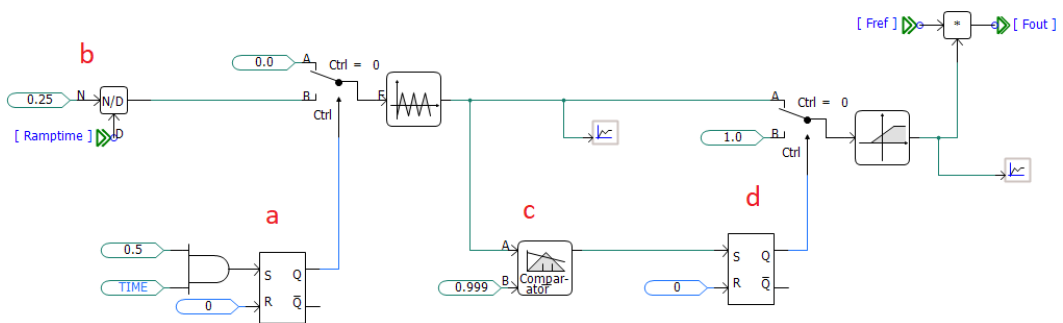

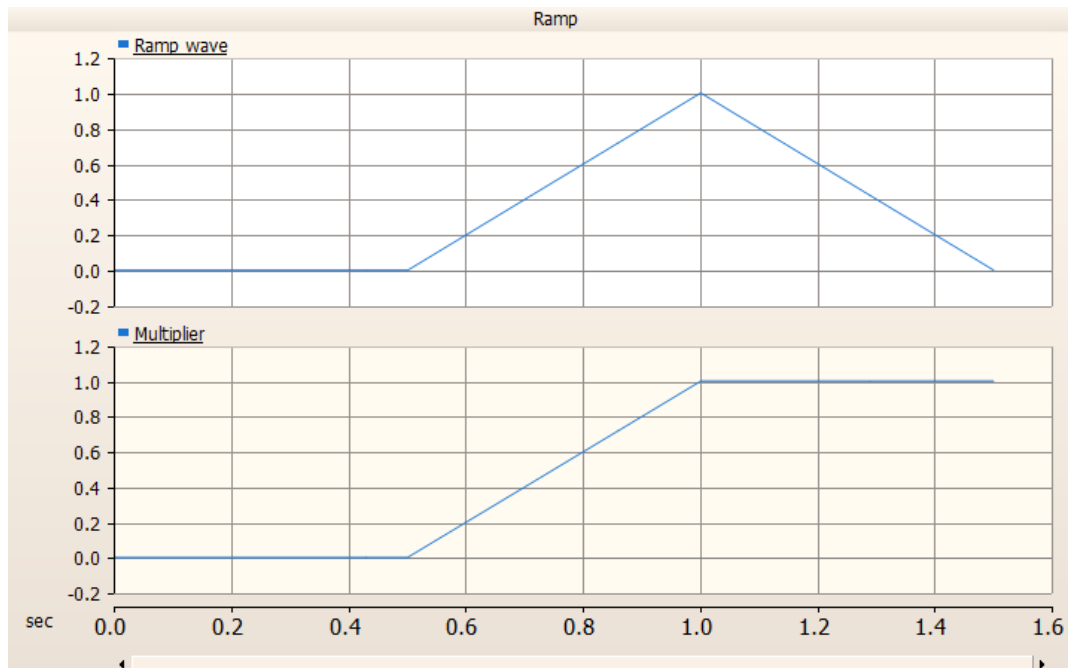**Figure 41.** Programmed acceleration ramp-logic.

Figure 42. The triangular wave used to program the acceleration ramp and the reference frequency multiplier.

In addition to the acceleration ramp, it would be a good idea to add V/f control to the frequency converter model as well in order to make the results as accurate as possible. With V/f control, the output voltage of a frequency converter is lower at lower frequencies during the ramp. The ratio of voltage to frequency during this control is linear. With the current drive model, the output voltage between two phases and the effect of the acceleration ramp on the output are shown in Figure 43.
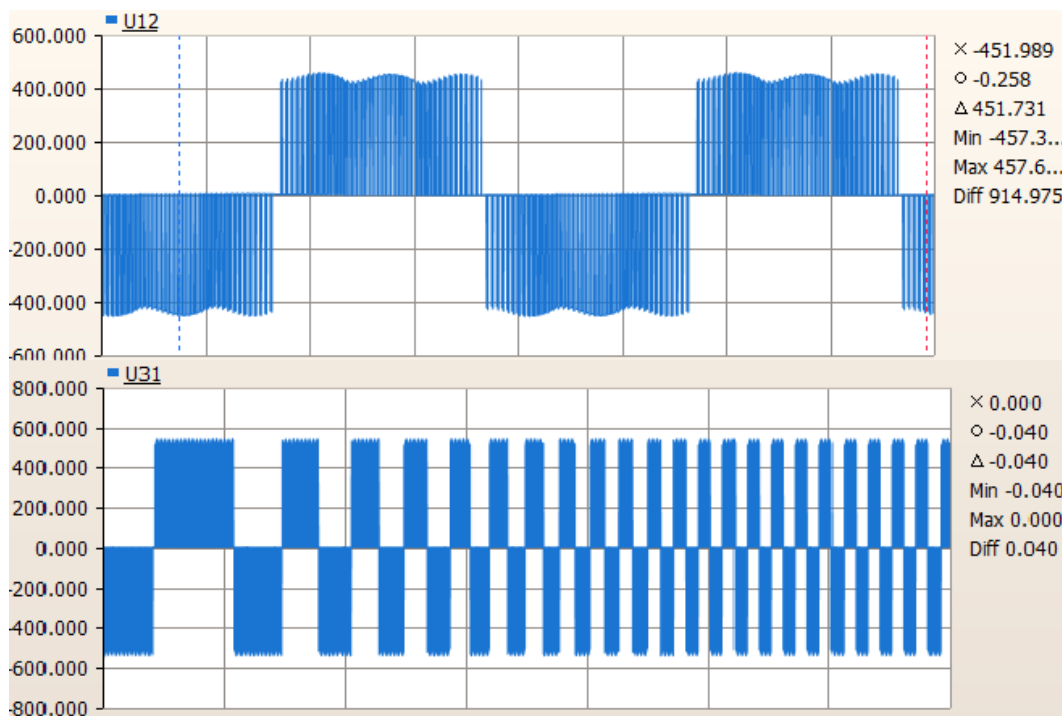
Figure 43. Output voltage and acceleration ramps effect on the output voltage of the new frequency converter simulation model (no V/f control).

This frequency converter model was also briefly used to simulate the WDR-60-5 models. Without using the simulated ramping logic, the DC side voltage and input current to WDR-60-5 were very similar to the PWM voltage used previously. When using the acceleration ramp, these values received a large transient at the end of the ramp. This could be corrected by adding V/f control to the simulation and improving the model further.

8   SUMMARY

To sum up the thesis, this approach on the selected device does not work directly. The project taught that the reference frequency of a frequency converter cannot be considered as the input circuit for electronics. Instead, the switching frequency should be used as the input frequency when designing the circuitry. It may be possible to make the power supply used in this project to work when connected to a motor, but this requires its input circuit to be redesigned for a frequency range of 1 kHz to 16 kHz instead of the 47 Hz to 63 Hz range.

The thesis presents directive ideas for redesigning and developing the input circuit. After designing the new input circuit, the simulations and tests presented in this thesis should be repeated with the redesigned device. Alternatively, the WDR-60-5 power supply could be replaced by another power source, or a completely new device could be designed with another input method. Additionally, an improved and more realistic frequency converter model is presented in the thesis for further research.

REFERENCES

/1/ History of ABB. ABB websites. Accessed 13.04.2021. https://global.abb/group/en/about/history

/2/ Our Businesses. ABB websites. Accessed 13.04.2021. https://new.abb.com/about/our-busines-ses?_ga=2.93562909.1247014836.1618245516-1637760202.1615463045

/3/ Suomalaiset juuret. ABB lyhyesti. ABB:n verkkosivut. Accessed 13.04.2021. https://new.abb.com/fi/abb-lyhyesti/historia/suomalaiset-juuret

/4/ Strömberg (yritys). Wikipedia. Accessed 13.04.2021. https://fi.wikipe-dia.org/wiki/Str%C3%B6mberg_(yritys)

/5/ Erturk, A. & Inman, D.J. 2011. Piezoelectric Energy Harvesting. John Wiley & Sons, Incorporated. s1-7.

/6/ Song, M-E., Yan, Y., Gollapudi, S., Bichurin, M., Petrov, V., Sanghadasa, M. & Priya, S. 2016. Design of Metglas/Polyvinylidene Fluoride Magnetoelectric Lami-nates for Energy Harvesting from Power Cords. IEEE. Accessed 02.04.2021. https://ieeexplore.ieee.org/document/7808818

/7/ Ahola, J., Ahonen, T., Särkimäki, V., Kosonen, A., Tamminen, J., Tiainen, R. & Lindh, T. 2008. Design Considerations for Current Transformer Based Energy Har-vesting for Electronics Attached to Electric Motor. IEEE. Accessed 03.04.2021. https://ieeexplore.ieee.org/document/4581191

/8/ Voltage transformer. Wikipedia. Accessed 05.04.2021. https://en.wikipe-dia.org/wiki/Voltage_transformer#Types_of_Voltage_Transformers

/9/ Universal Serial Bus Specification. Revision 2.0. USB.org. 2000. s175. https://usb.org/document-library/usb-20-specification

/10/ Specifications. Mean Well websites. Accessed 10.04.2021. https://www.meanwell-web.com/en-gb/ac-dc-industrial-din-rail-power-supply-output-5vdc-wdr--60--5

/11/ Danci, A. ABB, Motors & Generators.

/12/ Manitoba Hydro. Wikipedia. Accessed 10.04.2021. https://en.wikipedia.org/wiki/Manitoba_Hydro

/13/ NTC-thermistor. Wikipedia. Accessed 12.04.2021. https://fi.wikipedia.org/wiki/NTC-termistori

/14/ NTC Thermistor Catalogue. THINKING ELECTRONIC INDUSTRIAL CO., LTD. Accessed 12.04.2021. https://www.thinking.com.tw/upload/product/files/NTC%20Thermistor-SCK%20Series.pdf
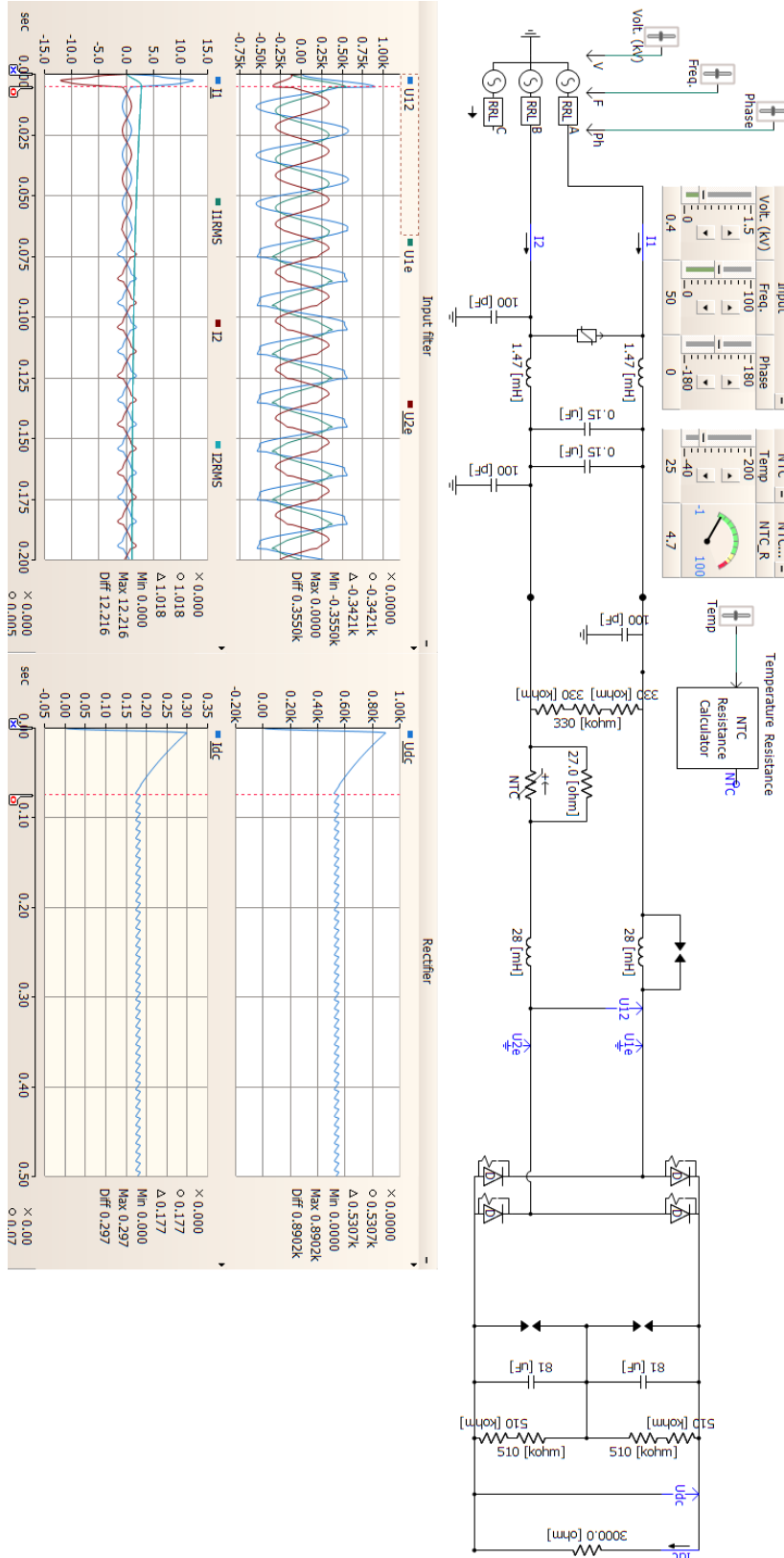
/15/ Sähköinfo Oy. 2017. D1-2017 Käsikirja rakennusten sähköasennuksista. Taulukko 41.6. s96.

/16/ Fuse-links. ESKA Erich Schweizer GmbH. Accessed 28.04.2021. https://www.starelec.fi/UserFiles/File/PDF-liitteet2/ESKA-520-500.pdf

/17/ Yang, Y. & Xiong, W. 2021. Extending the Supply Voltage of a 600V Input, No-Optocoupler Isolated Flyback Controller to 800V or Higher. Analog Devices websites. Accessed 01.05.2021. https://www.analog.com/media/en/technical-documentation/design-notes/extending-supply-voltage-600-v-input-no-optocoupler.pdf
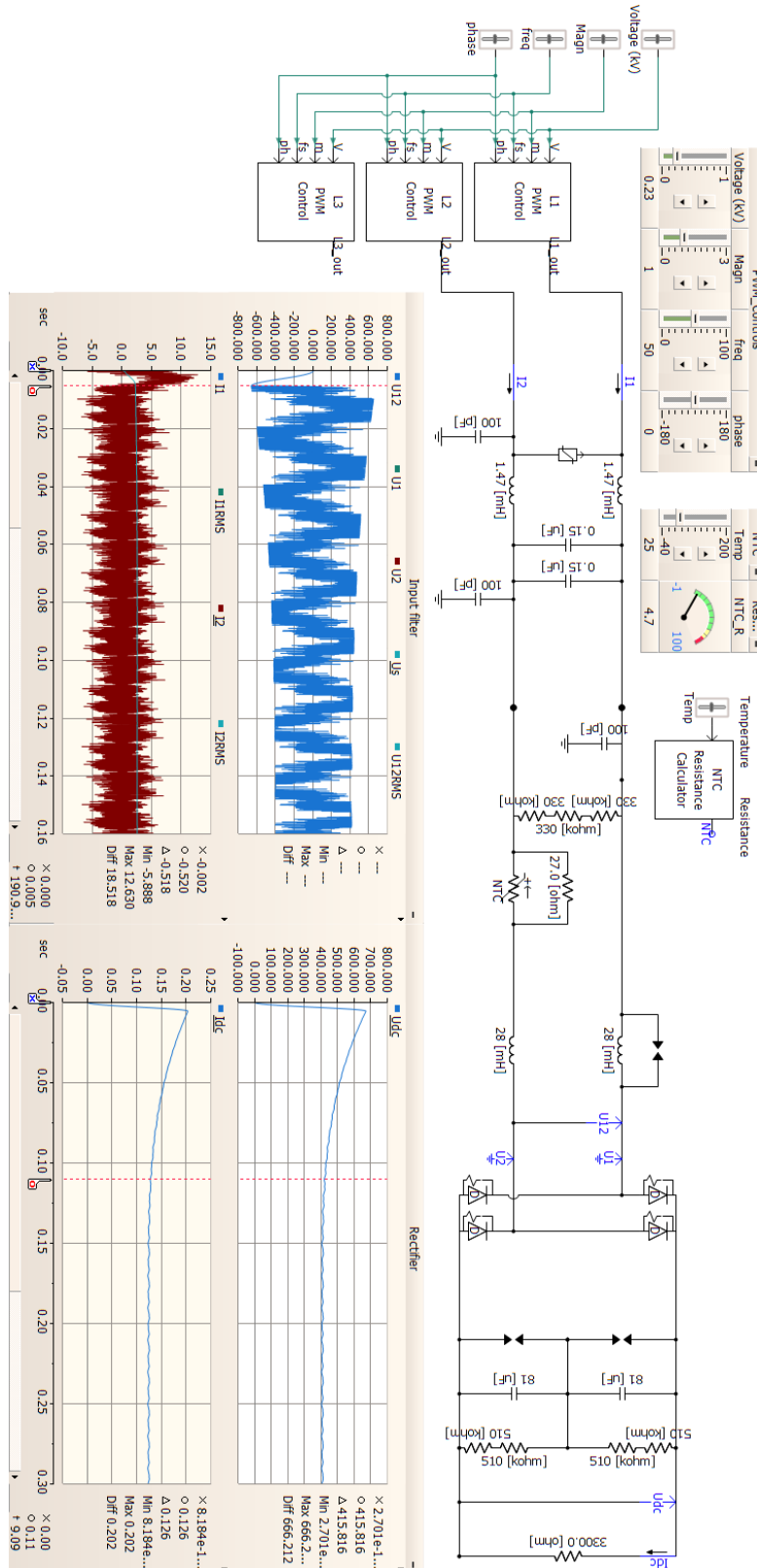
APPENDIX 1.

WDR-60-5 power supply fed with sine voltage.

APPENDIX 2.

WDR-60-5 power supply fed with a frequency converter.

APPENDIX 3.

WDR-60-5 power supply fed with a frequency converter, in parallel with a motor.

APPENDIX 4.

Simulated switching logic of the improved frequency converter.